

1 **Title**

2 Histology of type 3 macular neovascularization and microvascular anomalies in treated  
3 age-related macular degeneration: a case study

4 **Authors**

5 Andreas Berlin MD MS,<sup>1,2</sup> Diogo Cabral MD,<sup>3,4</sup> Ling Chen, MD PhD,<sup>1,5</sup> Jeffrey D  
6 Messinger DC,<sup>1</sup> Chandrakumar Balaratnasingam MD PhD,<sup>6-8</sup> Randev Mendis MD,<sup>9</sup>  
7 Daniela Ferrara MD PhD,<sup>10</sup> K. Bailey Freund MD,<sup>3,11</sup> Christine A Curcio PhD<sup>1\*</sup>

8

9 <sup>1</sup> Department of Ophthalmology and Visual Sciences, School of Medicine, University of  
10 Alabama at Birmingham, Birmingham AL, USA; <sup>2</sup> Department of Ophthalmology,  
11 University Hospital Würzburg, Würzburg, Germany; <sup>3</sup> Vitreous Retina Macula  
12 Consultants of New York NY, USA; <sup>4</sup> NOVA Medical School Research, Universidade  
13 NOVA de Lisboa, Portugal; <sup>5</sup> The First Affiliated Hospital of Chongqing Medical  
14 University, Chongqing Key Laboratory of Ophthalmology, and Chongqing Eye Institute,  
15 Chongqing, China; <sup>6</sup> Centre for Ophthalmology and Visual Science, University of  
16 Western Australia, Perth, Australia; <sup>7</sup> Lions Eye Institute, Nedlands, Western Australia,  
17 Australia; <sup>8</sup> Department of Ophthalmology, Sir Charles Gairdner Hospital, Western  
18 Australia, Australia; <sup>9</sup> Canberra Retina Center, Canberra Australia, <sup>10</sup> Genentech, South  
19 San Francisco, CA, USA; <sup>11</sup> Department of Ophthalmology, New York University  
20 Grossman School of Medicine, New York NY, USA

21

22 \*Corresponding author

23

24 **Short title** Intraretinal vascular morphologies in treated AMD

25 **Word count** 4007

26 **Figures** 11

27 **Tables** 2

28 **Supplementary** 5 figures, 1 video, 2 tables

29 **Corresponding Address**

30 Christine A. Curcio, PhD; Department of Ophthalmology and Visual Sciences; EyeSight

31 Foundation of Alabama Vision Research Laboratories; 1670 University Boulevard Room

32 360; University of Alabama at Birmingham, School of Medicine; Birmingham AL 35294-

33 0099; Email: [christinecurcio@uabmc.edu](mailto:christinecurcio@uabmc.edu)

34 **Key words**

35 age-related macular degeneration, type 3 macular neovascularization, deep retinal age-

36 related microvascular anomalies, vascular morphology, optical coherence tomography

37 angiography, histopathology, electron microscopy.

38

39

## Intraretinal vascular morphologies in treated AMD

### 40 **Abstract**

### 41 **Objective/Purpose**

42 To investigate intraretinal neovascularization and microvascular anomalies by correlating  
43 in vivo multimodal imaging with corresponding ex vivo histology in a single patient.

### 44 **Design**

45 A case study comprising clinical imaging from a community-based practice, and  
46 histologic analysis at a university-based research laboratory (clinicopathologic  
47 correlation).

### 48 **Participants**

49 A white woman in her 90's treated with numerous intravitreal anti-vascular endothelial  
50 growth factor (VEGF) injections for bilateral type 3 macular neovascularization (MNV)  
51 secondary to age-related macular degeneration (AMD).

### 52 **Intervention(s)/ Methods**

53 Clinical imaging comprised serial infrared reflectance, eye-tracked spectral-domain  
54 optical coherence tomography (OCT), OCT angiography, and fluorescein angiography.  
55 Eye tracking, applied to the two preserved donor eyes, enabled correlation of clinical  
56 imaging signatures with high-resolution histology and transmission electron microscopy.

### 57 **Main Outcome(s) and Measure(s)**

58 Histologic/ ultrastructural descriptions and diameters of vessels seen in clinical imaging.

### 59 **Results**

60 Six vascular lesions were histologically confirmed (type 3 MNV, n=3; deep retinal age-  
61 related microvascular anomalies (DRAMA), n=3). Pyramidal (n=2) or tangled (n=1)  
62 morphologies of type 3 MNV originated at the deep capillary plexus (DCP) and extended  
63 posteriorly to approach without penetrating persistent basal laminar deposit. They did  
64 not enter the sub-retinal pigment epithelium (RPE)-basal laminar space or cross Bruch's  
65 membrane. Choroidal contributions were not found. The neovascular complexes

## Intraretinal vascular morphologies in treated AMD

66 included pericytes and non-fenestrated endothelial cells, within a collagenous sheath  
67 covered by dysmorphic RPE cells. DRAMA lesions extended posteriorly from the DCP  
68 into the Henle fiber and the outer nuclear layers, without evidence of atrophy, exudation,  
69 or anti-VEGF responsiveness. Two DRAMA lacked collagenous sheaths. External and  
70 internal diameters of type 3 MNV and DRAMA vessels were larger than comparison  
71 vessels in the index eyes and in aged normal and intermediate AMD eyes.

### 72 **Conclusions**

73 Type 3 MNV vessels reflect specializations of source capillaries and persist during anti-  
74 VEGF therapy. The collagenous sheath of type 3 MNV lesions may provide structural  
75 stabilization. If so, vascular characteristics may be useful in disease monitoring in  
76 addition to fluid and flow signal detection. Further investigation with longitudinal imaging  
77 before exudation onset will help determine if DRAMA are part of the type 3 MNV  
78 progression sequence.

79

80

### 81 **Abbreviations**

82 AMD, age-related macular degeneration; BLamD, basal laminar deposit; BrM, Bruch's  
83 membrane; ChC, choriocapillaris; Ch, choroid; DCP, deep capillary plexus; DRAMA,  
84 deep retinal age-related microvascular anomalies; ELM, external limiting membrane;  
85 ETDRS, Early Treatment Diabetic Retinopathy Study; FA, fluorescein angiography; GCL,  
86 ganglion cell layer; HFL, Henle fiber layer; INL, inner nuclear layer; IPL, inner plexiform  
87 layer; IS, inner segment; MNV, macular neovascularization; nvAMD, neovascular age-  
88 related macular degeneration; OCT, optical coherence tomography; OCTA, optical  
89 coherence tomography angiography; ONL, outer nuclear layer; OPL, outer plexiform  
90 layer; OS, outer segment; RPE, retinal pigment epithelium.

91

## Intraretinal vascular morphologies in treated AMD

### 92 **Introduction**

93 Type 3 macular neovascularization (type 3 MNV) is a subtype of neovascular age-  
94 related macular degeneration (AMD).<sup>1</sup> Unlike type 1 MNV, which arises from the choroid,  
95 type 3 MNV originates in the neurosensory retina.<sup>2, 3</sup> Female gender, older age, and  
96 presence of subretinal drusenoid deposits confer risk for type 3 MNV.<sup>4, 5</sup> Type 3 MNV is  
97 diagnosed in a third of Caucasian patients presenting with unilateral neovascular AMD<sup>6</sup>  
98 and may be underestimated overall. Fellow eyes often convert to neovascular AMD  
99 within 3 years.<sup>7-9</sup> Early lesions respond well to intravitreal anti-vascular endothelial  
100 growth factor (VEGF) therapy, unlike chronic lesions.<sup>2, 10</sup> New information about type 3  
101 MNV and related vascular anomalies from histopathology, as provided herein, could  
102 support improved detection and treatment decisions in affected patients.

103 Recent clinical imaging studies have elucidated type 3 MNV pathophysiology.  
104 Three stages are defined based on structural optical coherence tomography (OCT).  
105 Precursors to Stage 1 are hyperreflective foci (HRF) at the level of the deep capillary  
106 plexus (DCP), often near drusen. Stage 1 includes an intraretinal hyperreflective lesion  
107 and cystoid macular edema. In Stage 2, outer retinal disruption appears. At Stage 3, the  
108 hyperreflective lesion extends into the sub-RPE basal lamina (BL) space, associated  
109 with a pigment epithelium detachment.<sup>2</sup> By color fundus photography, fluorescein  
110 angiography (FA), and OCT, type 3 MNV exhibit a specific regional distribution and  
111 pattern of hemorrhage.<sup>11-13</sup> Lesions localize preferentially to the inner ring of the Early  
112 Treatment of Diabetic Retinopathy Study (ETDRS) grid. Flame-shaped intraretinal  
113 hemorrhages are located over type 3 MNV lesions, pointing toward the fovea. OCT  
114 angiography (OCTA) with 3-dimensional reconstruction and display shows vertically  
115 oriented components of type 3 MNV. Using this technology, Borelli et al describe two  
116 morphologic phenotypes ('filiform' and 'saccular') of advanced type 3 MNV.<sup>14</sup>

## Intraretinal vascular morphologies in treated AMD

117 Prior clinicopathological correlation has elucidated some cellular detail  
118 corresponding to the OCT-based stages.<sup>15, 16</sup> Neovascular complexes originating at the  
119 DCP have a vertical and downward trajectory. These complexes expand posteriorly and  
120 cross persistent basal laminar deposit (BLamD) to enter the sub-RPE-BL space. Some  
121 complexes appear like base-down pyramids that are ensheathed by collagenous  
122 material.<sup>3, 16</sup> Participatory cells include macrophages, VEGF-positive fibroblasts,  
123 lymphocytes, Müller cell processes, and subducted RPE cells.<sup>15, 16</sup> Hence, ischemia and  
124 inflammation may promote the development and progression of type 3 MNV.<sup>15, 16</sup>

125 Microvascular abnormalities involving the DCP include microaneurysms,  
126 telangiectasia, perifoveal exudative anomalous vascular complex (PEVAC), and capillary  
127 macroaneurysms.<sup>17-22</sup> PEVAC was initially described in non-AMD eyes as an isolated  
128 aneurysmal dilation of a retinal capillary originating between the superficial and deep  
129 plexuses, with exudation that is unresponsive to anti-VEGF.<sup>17, 22, 23</sup> Deep retinal age-  
130 related microvascular anomalies (DRAMA) are recently proposed as DCP alterations in  
131 the setting of AMD findings like soft drusen and intraretinal HRF. Eyes with DRAMA  
132 show abnormal horizontal or vertical vessels with a diameter of >50  $\mu\text{m}$  and/or a location  
133 below the posterior border of the outer plexiform layer (OPL).<sup>24</sup> In contrast to type 1  
134 MNV,<sup>25</sup> precursors, early stages, and potential masqueraders for type 3 MNV, which  
135 may include DRAMA, are not described at the histologic level.<sup>26</sup> Human eyes with  
136 longitudinal clinical imaging are especially valuable sources for such information.<sup>3</sup>

137 Herein we directly compared longitudinal OCT and angiographic signatures of  
138 intraretinal neovascularization and microvascular anomalies to corresponding histology.  
139 We analyzed both eyes of a single patient who had received intravitreal anti-VEGF  
140 treatments for type 3 MNV over the course of 5 years (right eye) and 9 months (left eye).

141

142

## Intraretinal vascular morphologies in treated AMD

### 143 **Methods**

#### 144 Compliance

145 Approval for this study was obtained by Institutional review at the University of  
146 Alabama at Birmingham (protocol #300004907). The study was conducted in  
147 accordance with the tenets of the Declaration of Helsinki and the Health Insurance  
148 Portability and Accountability Act of 1996.<sup>27, 28</sup>

#### 149 Clinical course

150 A white, pseudophakic woman in her 90's received comprehensive  
151 ophthalmologic examination and multimodal imaging during a 5-year follow-up for  
152 bilateral type 3 MNV secondary to AMD. The patient presented 5 years prior to death  
153 with exudative type 3 MNV in the right eye. Over 5 years, she received a total of 37  
154 intravitreal anti-VEGF injections over approximately 6 fluid resorption cycles in the right  
155 eye (12 x 0.5 mg/ 0.05 ml ranibizumab then 25 x 2 mg/ 0.05 ml aflibercept). One fluid  
156 resorption cycle is defined as the time in weeks and the number of injections needed  
157 from initial detection of intraretinal/ subretinal edema on OCT until complete absence of  
158 edema on OCT. The left eye was diagnosed with exudative type 3 MNV 4 years after the  
159 right eye. Over 9 months, the left eye received a total of 6 intravitreal anti-VEGF  
160 injections over approximately 2 fluid resorption cycles (12 x 0.5 mg/ 0.05 ml  
161 ranibizumab). Her general medical history included dyslipidemia and paroxysmal atrial  
162 fibrillation. Six months before death, the patient was diagnosed with gallbladder  
163 adenocarcinoma. Her last anti-VEGF treatment before death due to adenocarcinoma  
164 was 3 and 2 months for the left and right eye, respectively.

#### 165 Clinical image capture and analysis

166 All images were acquired using Spectralis HRA+OCT (Heidelberg Engineering,  
167 Heidelberg, Germany). Available for review were 11 (right eye) and 7 (left eye) eye-

## Intraretinal vascular morphologies in treated AMD

168 tracked spectral domain OCT volumes (6 mm x 6 mm horizontal and radial scans; 20° x  
169 20° field). FA was available for both eyes at first presentation and 4 years later.  
170 One eye-tracked spectral domain OCTA volume (3 mm x 3 mm horizontal scans, 256 B-  
171 scans at 6 µm spacing, 10° x 10° field, ART 5, quality 34 dB) was obtained of the right  
172 eye 3.5 years after presentation.<sup>29</sup> An investigational version of Heidelberg Eye Explorer  
173 (v. 6.16.100.701, Heidelberg Engineering, Heidelberg, Germany) was used for analysis,  
174 processing, and post-processing of data.<sup>3,30</sup> Projection artifact was removed via 3-  
175 dimensional vessel-shape estimation and a Gaussian blur filter.<sup>3, 30</sup> Raw (floating point)  
176 data were exported as a .VOL file.

177 Volume rendering enhances visualization of type 3 MNV, which is vertically  
178 oriented, and allows afferent/ efferent vascular connections to be identified, particularly  
179 in deeper retinal layers.<sup>3, 31</sup> To visualize lesions at different angles of rotation, OCTA B-  
180 scans were first processed using linear quadratic estimation (noise variance estimate of  
181 0.05 and a gain of 0.8; MATLAB version R2019b, Natick, Massachusetts: The  
182 MathWorks Inc.; 2019), followed by volume rendering and analysis (Imaris v9.5, Bitplane,  
183 Andor Technology plc.).<sup>32</sup> The Filament Tracer tool was used to trace superficial arteries  
184 and veins after evaluation of dye circulation in FA. Video recording and still images were  
185 annotated to highlight structural and flow details.

186 Previous reports indicated both eccentricity- and hemifield-dependent  
187 asymmetries in the spatial distribution of type 3 MNV.<sup>11, 12, 33</sup> Thus, for potential  
188 mechanistic insight into tissue-level associations, location of vascular lesions was  
189 documented. Lesion distance from the fovea was calculated using the OCT volume and  
190 NIR en face image using a custom ImageJ plug-in 'Spectralis Browser OCT', available at  
191 <https://sites.imagej.net/CreativeComputation/>. Meridional position was documented  
192 using the sectors of the ETDRS grid.<sup>34,35</sup>



## Intraretinal vascular morphologies in treated AMD

193

### 194 Histology preparation and image analysis

195 As described,<sup>36</sup> globes were recovered 2:05 hours after death and preserved in  
196 buffered 1% paraformaldehyde and 2.5% glutaraldehyde. Pre-mortem eye-tracked OCT  
197 volumes were registered to post-mortem OCT volumes of the same globes.<sup>37</sup> For high-  
198 resolution histology over large areas, a rectangular tissue block containing fovea and  
199 optic nerve was post-fixed in 1% osmium – tannic acid – paraphenylenediamine and  
200 embedded in epoxy resin. A tissue block 8 mm x12 mm wide was processed for stepped  
201 sections at 30-60  $\mu\text{m}$  intervals. Interleaved 30  $\mu\text{m}$ -thick slabs were re-embedded for  
202 transmission electron microscopy (TEM). Sub-micrometer sections stained with toluidine  
203 blue were scanned using a 60X oil immersion objective.<sup>38</sup> Tissue sections on 112 (right  
204 eye) and 87 (left eye) glass slides spanning a distance of 5453  $\mu\text{m}$  (right eye) and 4243  
205  $\mu\text{m}$  (left eye) centered on the two foveas were matched to clinical OCT scans by  
206 comparing overall tissue contours.

207 DRAMA vessels are defined by a diameter criterion ( $>50 \mu\text{m}$ ),<sup>24</sup> and our previous  
208 and current observations indicated that a collagenous sheath surrounds type 3 MNV  
209 neovessels. Further, OCTA shows only the moving blood cell column and not the  
210 collagenous sheath. Therefore, we manually measured internal (luminal) and external  
211 cross-sectional diameters of vessels ('oval' tool, FIJI Is Just; ImageJ 2.0.0-rc- 69/1.52p;  
212 [www.fiji.sc](http://www.fiji.sc));). Type 3 MNV vessels meandered over several glass slides, and sections on  
213 each slide were measured. To contextualize neovessel measurements, DCP vessels on  
214 either side of the area directly involved in exudation in the index case were also  
215 measured. Further, vessels aligned along the outer border of the INL of intermediate  
216 AMD eyes and age-similar controls (n= 8 each) on the Project MACULA website of AMD  
217 histopathology were also measured.<sup>25</sup> Because vessels could run longitudinally within a

## Intraretinal vascular morphologies in treated AMD

218 section, we report a minimal cross-section diameter (approximated by Feret diameter in  
219 ImageJ for ellipses). Due to small numbers, these data were not analyzed statistically.  
220

## Intraretinal vascular morphologies in treated AMD

### 221 **Results**

222 **Table S1** lists all figures to provide an overview.

#### 223 Classification of lesions and longitudinal clinical imaging

224 We first classify vascular complexes in the two eyes at one time point, then  
225 describe them in longitudinal clinical imaging and detailed histology. **Table 2** lists  
226 hyperfluorescent lesions seen by FA 11 months before death (**Figure 1**). Six of 7 lesions  
227 localized to the inner ring of the ETDRS grid (0.5-1.5 mm eccentricity), with the seventh  
228 at 1.52 mm. There was no predilection for any one sector. Six of 7 lesions were  
229 confirmed as vascular by histology, and the seventh (**Figure S2**) could not be found.  
230 Lesion morphology was categorized as tangled type 3 MNV (n=1), pyramidal type 3  
231 MNV (n=2), or DRAMA (n=3). As seen previously,<sup>3, 16</sup> pyramidal type 3 MNV was  
232 defined as a focal, vertically extending neovessel complex. Tangled type 3 MNV was  
233 defined as a horizontally extending neovessel complex. DRAMA was defined as  
234 anomalous vascular elements extending posterior to the DCP and into the HFL/ONL, i.e.,  
235 anterior to the ELM.<sup>24</sup> Hyperfluorescent lesions in the right eye due to window defects  
236 were reported elsewhere.<sup>39</sup>

237 At initial presentation 5 years before death, the right eye exhibited multiple  
238 instances of MNV secondary to AMD with multifocal leakage on FA (**Figure S3**). At this  
239 time, fluid was not detected in the left eye (**Figure S4**). Four years later and 11 months  
240 before death (**Figure 1**), the left eye was diagnosed with exudative type 3 MNV due to  
241 AMD. By this time, the right eye had received 32 intravitreal anti-VEGF injections at  
242 intervals of 4-8 weeks resulting in 4 fluid resorption cycles.

#### 243 Pyramidal (OD 2, OS 4) and tangled (OD 1) type 3 MNV

244 Pyramidal type 3 MNV (OS 4) closely resembles previously described OD 2<sup>4</sup> in  
245 terms of location, OCT appearance, and histologic features (**Figure 1, Figure 5, Figure**  
246 **6**, respectively). In brief, OS 4 is a vertically oriented, pyramidal-shaped, intraretinal

## Intraretinal vascular morphologies in treated AMD

247 lesion located in the nasal sector of the ETDRS inner ring, with heterogeneous  
248 hyperreflectivity on OCT (**Figure 5**). On histology, this lesion corresponds to a collagen-  
249 ensheathed neovascular complex that extends from the OPL/INL border through the  
250 HFL /ONL (**Figure 6A**). The complex is flanked by RPE cells that extend off the top of  
251 the pyramid and along a DCP vessel (**Figure 6B**). The pyramid base adheres to  
252 denuded and persistent BLamD, which drapes a calcified druse (**Figure 6A&B**).<sup>4</sup> The  
253 vessel did not enter the subRPE-BL space, and no choroidal contribution was found.

254 Transmission electron microscopy of this pyramidal lesion reveals endothelial  
255 cells and pericytes (**Figure 7A**). Endothelial cells are not fenestrated (**Figure 7B**), like  
256 endothelial cells of the DCP and unlike endothelial cells of the choriocapillaris (**Figure**  
257 **7C&D**). Other vessel wall components, e.g., smooth muscle cells, connective tissue, or a  
258 3-layer arterial configuration, cannot be identified. In RPE cells arrayed along the sloping  
259 sides of the calcified druse, lipofuscin becomes less electron-dense, smaller, and less  
260 tightly packed (**Figure 7E**), in a smooth transition. These findings suggest  
261 transdifferentiation, rather than ingestion of RPE organelles by invading phagocytes.

262 Next we consider tangled type 3 MNV (OD 1), for which en face OCTA (**Figure**  
263 **8A2**) and OCT with flow overlay (**Figure 8A3**) shows persistent flow signal. Over time,  
264 the extent of intraretinal fluid surrounding OD 1 in the INL and HFL fluctuates (**Figure**  
265 **8B2, Figure 8C2**, respectively). Volume rendering of structural OCT and OCTA together  
266 highlights flow within a hyperreflective lesion at the ONL and bacillary layer (**Figure S9A,**  
267 **Video S1**). Inflow and outflow vessels can be connected to a superficial artery and vein,  
268 respectively (**Figure S9B&C**). The RPE/BrM complex below the lesion is split by  
269 hyporeflexive material producing a double layer sign (**Figure 7B2**).<sup>40</sup> Numerous HRF  
270 are present in the INL (**Figure 8C2**).

271 Histologic analysis reveals components of tangled type 3 MNV (OD 1, **Figure**  
272 **8D**). Magnified histology shows a vascular complex spanning 249  $\mu\text{m}$  horizontally,

## Intraretinal vascular morphologies in treated AMD

273 extending into the superior perifovea (**Figure S10**). The complex is partly ensheathed by  
274 collagenous material and flanked by intraretinal RPE cells. The INL/OPL border  
275 subsides where the vascular lesion extends through the HFL/ONL (**Figure S10C**). The  
276 ELM subsides at both edges of the calcified druse (yellow arrows in **Figure S10B**).  
277 Bruch's membrane appears intact without evidence of a choroidal contribution to the  
278 MNV lesions, or evidence of MNV contributing to the OCT double layer sign (**Figure**  
279 **S10A-C**). Neovessels within the INL are moderately dilated, suggesting drainage  
280 venules (**Figure S10A**).<sup>41</sup>

281 To summarize, vascular geometry and thickness of the collagenous sheath  
282 differentiates tangled versus pyramidal type 3 MNV. The sheath surrounding the tangled  
283 complex is thin (**Figure S10**), and that surrounding pyramidal type 3 MNV is thick  
284 (**Figure 6**). Otherwise, the two subtypes are comparable.

### 285 DRAMA, in the setting of anti-VEGF therapy

286 As shown below, all three instances of DRAMA (OS 1, OS 3, and OD 3) exhibit  
287 mild hyperfluorescence on venous and recirculation phase FA 11 months before death.  
288 In histology, all three localize above a horizontal ELM, signifying lack of atrophy.

289 OS 1 includes a vessel extending from the INL into the ONL (**Figure 11A**). Like  
290 type 3 MNV lesions, this DRAMA lesion is located above a soft druse with BLamD and  
291 altered RPE at its apex (**Figure 11C**). Unlike type 3 MNV, OS 1 does not have a  
292 collagenous sheath, and the OPL does not subside (**Figure 11C2**).

293 Corresponding to FA, OCT of OS 3 shows an intraretinal hyperreflective,  
294 stacked lesion, without intraretinal cysts (**Figure 12A**). Over time, a plume of HRF  
295 extends nasally, still without evidence of cysts (**Figure 12C**).<sup>42, 43</sup> In histology, an RPE  
296 tower atop a soft druse extends into the OPL (**Figure 12D**). This RPE complex  
297 surrounds like a gripping hand a vessel extending downward from the DCP (**Figure**  
298 **13A&B**). By light microscopy, the extending vessel in OS 3 resembles DRAMA OS 1

## Intraretinal vascular morphologies in treated AMD

299 (Figure 11) in its location above a soft druse with thick BLamD and a thinned RPE layer.  
300 By transmission electron microscopy, OS 3 (Figure S14) resembles type 3 MNV lesions  
301 but lacks a collagenous sheath. Endothelial cells in OS 3 lack fenestrations (Figure 13C),  
302 like endothelial cells of the DCP and unlike endothelial cells of the choriocapillaris  
303 (Figure 13D&E) Other vessel wall components cannot be identified. The RPE complex  
304 is multicellular, with some multinucleated cells (Figure S14). Organelle packing and  
305 electron density is similar to in-layer RPE cells (not shown).

306 OCTA flow overlay of DRAMA OD 3 shows an intraretinal hyperreflective lesion  
307 containing a pair of vascular outpouchings (Figure 15C). Corresponding histology  
308 displays a pair of deeply descending vessels without significant intraretinal fluid (Figure  
309 15D). Like type 3 MNV, the vessel complex of this DRAMA is ensheathed by a thin layer  
310 of collagenous material and dives from the INL into the HFL (Figure 16A). Unlike type 3  
311 MNV, the vessels do not extend past the HFL, and there is no subsidence of the ELM.  
312 RPE organelles appear near the vessel complex (Figure 16B).

### Vessel diameters of vascular lesions and comparison vessels

314 Table S3 shows internal and external vessel diameters of type 3 MNV and  
315 DRAMA, as well as DCP vessels in the index case and donor eyes (8 intermediate AMD,  
316  $83.4 \pm 11.6$  years; 8 controls,  $84.1 \pm 6.7$  years). Five of the 6 index case lesions are  
317 noticeably larger (2.5-3-fold) than the comparison vessels. External vessel diameters of  
318 type 3 MNV (OD 1,  $15.02 \mu\text{m} \pm 3.81 \mu\text{m}$ ; OD 2,  $21.35 \mu\text{m} \pm 10.79 \mu\text{m}$ ; OS 4  $12.46 \mu\text{m} \pm$   
319  $0.95 \mu\text{m}$ ) are larger than nearby DCP diameters ( $7.18 \mu\text{m} \pm 1.11 \mu\text{m}$ ). They are also  
320 larger than vessel diameters in intermediate AMD ( $6.79 \mu\text{m} \pm 1.05 \mu\text{m}$ ) and control ( $7.86$   
321  $\mu\text{m} \pm 1.47 \mu\text{m}$ , Table S3A) eyes. In DRAMA, external vessel diameters of OS 1 and OS  
322 3 ( $13.39 \mu\text{m} \pm 2.68 \mu\text{m}$ ;  $17.97 \mu\text{m} \pm 1.08 \mu\text{m}$ ) are considerably larger than the  
323 comparison vessels. A similar pattern is seen for internal vessel diameters (Table S3B).

## Intraretinal vascular morphologies in treated AMD

324 An overview of unifying and distinguishing features of type 3 MNV and DRAMA,

325 combining this and prior reports, is provided in **Table 4**.<sup>3, 16, 24</sup>

326

327

## Intraretinal vascular morphologies in treated AMD

### 328 **Discussion**

329           In two anti-VEGF treated eyes of one patient with neovascular AMD, we compare  
330 longitudinal multimodal clinical imaging and histology of type 3 MNV and DRAMA (**Table**  
331 **2, Table 4**). Although one patient, the clinical and imaging characteristics are typical of  
332 multifocal type 3 MNV, including bilaterality (55% of cases)<sup>44</sup> and absence of type 1  
333 MNV.<sup>11-13, 44, 45</sup> Type 3 MNV is distinguished by intraretinal origin,<sup>1, 2, 46</sup> frequent near-term  
334 bilateral involvement,<sup>7-9</sup> and significant choroidal thinning with reduced perfusion.<sup>47, 48</sup>  
335 Patients with type 3 MNV are older at initial diagnosis than patients with type 1 MNV.<sup>49, 50</sup>

336           In our case, treated type 3 MNV has two morphologic phenotypes, pyramidal (OD  
337 2, OS 4) or tangled (OD 1). All three analyzed complexes originate at the DCP and  
338 extend posteriorly to approach persistent BLamD but do not enter the sub-RPE-BL  
339 space or cross BrM. These two phenotypes may correspond to those seen by Borelli et  
340 al in treatment-naïve type 3 MNV eyes with rotational three-dimensional OCTA. These  
341 authors describe 26 lesions as ‘filiform’ and 9 lesions as ‘saccular’, which appear similar  
342 in shape to pyramidal (filiform) and tangled (saccular).<sup>14</sup> We also find more pyramidal  
343 lesions than tangled. It remains to be determined if saccular and filiform lesions differ in  
344 spatial distribution and time of onset.<sup>14</sup>

345           Our previous description of pyramidal Type 3 MNV included endothelial cells in a  
346 thick collagenous matrix and dysmorphic RPE cells scattered along the neovascular  
347 stalk.<sup>16</sup> OD2 and OS4 in this case<sup>3</sup> add pericytes plus a nearly continuous covering by  
348 highly pigmented RPE (OS4), supporting the early involvement of migratory RPE.<sup>2, 51</sup>  
349 The sheath distinguishes lesions from unaffected DCP vessels. The main differences  
350 between pyramidal and tangled lesions are the larger horizontal extent and thinner  
351 collagenous sheath of tangled.<sup>3</sup> Endothelial cells of tangled vessels, and presumably  
352 also those in pyramidal, lack fenestrations like the source vessels in the DCP.



## Intraretinal vascular morphologies in treated AMD

353 As before,<sup>16</sup> we did not see vessels of choroidal origin in the sub-RPE-BL space,  
354 as reported for advanced type 3 MNV.<sup>14, 44, 52-54</sup> Nor did we see DCP-originating vessels  
355 penetrate through BLamD and enter the sub-RPE- BL space. This depth of penetration  
356 was suggested as necessary for exudation.<sup>55</sup> This proposal was based on OCTA  
357 imaging without projection artifact removal to reduce spurious signal directly under type  
358 3 MNV.<sup>55</sup> Using volumetric artifact removal, we did not see OCTA flow signal in the sub-  
359 RPE-BL space (**Figure 8A3**). It is possible that anti-VEGF treatment rendered invisible  
360 downward projections from the DCP or upward projections from the choriocapillaris. We  
361 think this is unlikely, because neo-capillaries may shrink after treatment, but they do not  
362 disappear.<sup>56, 57</sup> Further, our use of stepped sections may miss key details. Nevertheless,  
363 in all analyzed sections of this case, both BLamD and BrM were intact. Longitudinal  
364 imaging before exudation onset is needed to understand this phase of type 3 MNV  
365 progression.

366 The thick collagenous sheath of type 3 MNV lesions may impact clinical  
367 monitoring, as follows. All lesions responded to anti-VEGF with temporary resolution of  
368 exudation and persistence over several fluid absorption cycles. By OCTA, some early-  
369 stage lesions regress completely while treatment of later-stage lesions require  
370 continuing therapy.<sup>2, 54</sup> Further, treated type 3 MNV lesions can reappear after becoming  
371 undetectable on OCTA.<sup>55, 58</sup> Lesions with thick sheaths remain detectable by structural  
372 OCT long after treatment.<sup>57</sup> The collagenous neovascular stalk was populated by  
373 endothelial cells and pericytes that either remained, self-renewed, or migrated in during  
374 VEGF cycles. We can speculate that the sheath structurally stabilizes endothelial cells  
375 within it and that both VEGF and anti-VEGF agents impact lesions principally where the  
376 sheath is absent. If MNV persistence after treatment, as well as recurrence after

## Intraretinal vascular morphologies in treated AMD

377 apparent regression, is influenced by sheaths, then monitoring for disease activity by  
378 vascular characteristics in addition to fluid may be useful.

379 We showed that type 3 MNV can coexist with vascular formations that are  
380 candidate precursors, early stages, and masqueraders for type 3 MNV. All three  
381 DRAMA originated from the DCP and extended posteriorly into the HFL. None of the  
382 DRAMA lesions involved the superficial capillary plexus, and no significant intraretinal  
383 fluid was detectable on OCT over time. Like type 3 MNV (**Figure 10**), one DRAMA had  
384 non-fenestrated endothelial cells and pericytes (**Figure S14**). Unlike type 3 MNV and like  
385 native DCP, two DRAMA lacked a collagenous sheath. The one DRAMA with a thin  
386 sheath (OD 3) also extended furthest of the three into the ONL, perhaps indicating  
387 chronicity. Importantly, none of the DRAMA were accompanied by descent of the ELM,  
388 the border of atrophy in neurosensory retina, although the ELM can be perforated by  
389 inwardly migrating RPE as in OS 3. It is unlikely that DRAMA in our case represent  
390 exudative or non-exudative perifoveal vascular anomalous complexes (ePVAC/  
391 nePEVAC),<sup>31,35,36</sup> which typically appear above the DCP. Microvascular anomalies in  
392 eyes with neovascular and non-neovascular AMD include capillary dilations and  
393 telangiectasia that are associated with locally increased VEGF expression.<sup>17,59-61</sup> A  
394 recent study showed that 19/94 eyes with type 3 MNV exhibited an asymptomatic  
395 precursor stage on OCT.<sup>44</sup> Because lack of exudation and non-progression to type 3  
396 MNV in our case might result from VEGF suppression,<sup>62</sup> longitudinal imaging is required  
397 to definitively place DRAMA in the progression sequence of type 3 MNV.

398 All analyzed vessels localized within 500-1500  $\mu\text{m}$  of the foveal center, aligned  
399 with similar findings for solitary and multifocal lesions.<sup>11, 12</sup> A role for choroidal ischemia  
400 is hypothesized,<sup>11, 63-65</sup> because the choroid is thinner in eyes with type 3 MNV than in  
401 eyes with types 1 and 2 MNV.<sup>66, 67</sup> The radial symmetry of lesions around and close to  
402 the fovea further suggests an association with the distribution of photoreceptors and

## Intraretinal vascular morphologies in treated AMD

403 their support cells, which vary markedly in this eccentricity range. The ETDRS inner ring  
404 of type 3 MNV vulnerability is just peripheral to the foveal avascular zone<sup>33</sup> on the inner  
405 slope of the crest of high rod density. Rod vision in AMD eyes is poorest in the same  
406 area.<sup>68-72</sup> Metabolic demand of foveal cones is high, and choriocapillaris OCTA signal  
407 decreases under the fovea throughout adulthood.<sup>73, 74</sup> It is thus possible that the  
408 distribution of type 3 MNV is an additional effect of microvascular changes under the  
409 fovea that also contribute to high-risk drusen and reduced sustenance of nearby rods.

410 Study strengths include the availability of OCTA with eye-tracked OCT,  
411 volumetric projection artifact removal, rapid tissue preservation to largely maintain retinal  
412 attachment, registration of pre-mortem and post-mortem OCT volumes, and  
413 comprehensive histologic and microscopy techniques to reveal vessels and perivascular  
414 tissue elements. Limitations include the lack of longitudinal OCTA imaging<sup>9, 75</sup> and lack  
415 of color fundus photography to reveal discoloration patterns typical of type 3 MNV.<sup>14</sup>  
416 Limitations to the laboratory study included use of stepped sections, lack of electron  
417 microscopy for all lesions, and lack of immunohistochemistry to support cell type  
418 identifications based on morphologic criteria. Finally, observations from one patient  
419 however detailed cannot elucidate the full range of biologic variability.

420 Nevertheless, our study helped define morphologies of type 3 MNV and  
421 proposed precursors that might guide future research, diagnosis, and disease monitoring.  
422 The presence and extent of a collagenous sheath distinguishes type 3 MNV from normal  
423 DCP vessels and may represent a stage in the evolution of DRAMA toward type 3 MNV.  
424 Our hypotheses can be tested in the larger samples available in clinic populations and  
425 clinical trial imaging datasets, ideally before onset of exudation.

426

## Intraretinal vascular morphologies in treated AMD

### 427 **Acknowledgments**

428

### 429 **Contribution statement**

430 All authors were involved in drafting the article or revising it critically for important  
431 intellectual content, and all authors approved the final version to be published. Dr. Curcio  
432 and Dr. Berlin had full access to all the data in the clinical picture and take responsibility  
433 for the integrity of the data and the accuracy of the data analysis. Study conception and  
434 design: AB, DC, LC, CB, RM, DF, KBF, CC. Acquisition of data: RM, CB, JM, LC, AB,  
435 DC, KBF, CC. Analysis and interpretation of data: AB, DC, LC, DF, KBF, CC. Writing of  
436 manuscript: AB, DC, CB, LC, RM, DF, KBF, CC.

437

### 438 **Financial support**

439 This work was supported by Genentech/ Hoffman LaRoche, The Macula Foundation,  
440 Inc., New York, NY; unrestricted funds to the Department of Ophthalmology and Visual  
441 Sciences (UAB) from Research to Prevent Blindness, Inc., and EyeSight Foundation of  
442 Alabama. AB reports grants from the Dr. Werner Jackstädt-foundation. DC was  
443 supported in part by a studentship from Fundação Luso-Americana para o  
444 desenvolvimento (FLAD, USA R&D@PhD – Proj 2020/0140). Purchase of the slide  
445 scanner was made possible by the Carl G. and Pauline Buck Trust.

446 The sponsors had no role in the design and conduct of the study; collection,  
447 management, analysis, and interpretation of the data; preparation, review, or approval of  
448 the manuscript; and decision to submit the manuscript for publication.

449

## Intraretinal vascular morphologies in treated AMD

### 450 **Financial disclosure**

451 KBF is a consultant to Genentech, Zeiss, Heidelberg Engineering, Allergan, Bayer, and  
452 Novartis. CAC receives research funds from Regeneron (outside this project). DF is an  
453 employee of Genentech and a stockholder of Roche.

454

### 455 **Meeting presentation**

456 This work was submitted as part of an abstract to the annual meeting of The Association  
457 for Research in Vision & Ophthalmology (ARVO) May 2021 and May 2022.

458

459

460

461

462

## Intraretinal vascular morphologies in treated AMD

### 463 **Figures**

#### 464 **Figure 1. Multimodal retinal imaging of both eyes, 11 months before death.**

465 **A & D.** Fluorescein angiography (FA) in venous (**A**) and recirculation phases (**D**) shows  
466 multiple instances of hyperfluorescence. Vessels were found by histology at the green,  
467 yellow, and fuchsia arrowheads in the right (**A**), and left eye (**D**). At the white arrowhead  
468 in the left eye, no vessel could be found in histology.

469 **B & E.** Near-infrared reflectance imaging (NIR) shows reduced reflectance in areas of  
470 angiographic leakage (arrowheads), possibly due to retinal edema. Soft drusen exhibit  
471 hypo- and hyperreflective mottling. Scale bar 200  $\mu\text{m}$ .

472 **C & F.** Fundus autofluorescence (FAF;  $\lambda_{\text{ex}}=488\text{ nm}$ ) highlights subretinal drusenoid  
473 deposits especially superior to the fovea.

474 Lesion number, type, and spatial distribution are listed in [Table 2](#).

475

#### 476 **Figure S2. Hyperfluorescence without histologic correlate, OS 2**

477 **A.** Fluorescein angiography (FA, **A1**) venous phase, 11 months before death, shows  
478 multiple instances of hyperfluorescence. An optical coherence tomography (OCT) B-  
479 scan (green line) displays drusen, a double-layer sign (white arrowhead), choroidal  
480 hypertransmission, and hyperreflective foci (**A2**).

481 **B, C.** At 4 and 2 months before death, with 5 (**B**) and 6 (**C**) total injections, respectively,  
482 the lesion is stable, without intraretinal cysts.

483

#### 484 **Figure S3. Initial presentation of right eye, 5 years before death**

485 **A-E.** Fluorescein angiography (FA), near infrared reflectance images (NIR), and radial  
486 optical coherence tomography (OCT) B-scans show exudative age-related macular  
487 degeneration in the right eye at initial presentation. Based on these findings anti-VEGF  
488 therapy is initiated.

489 **A.** FA recirculation phase shows marked leakage. Corresponding OCT shows  
490 intraretinal and subretinal hyporefective cysts and spaces representing exudation,  
491 located above drusenoid pigment epithelium detachments in the fovea and parafovea.

492 **B.** NIR and OCT show hyporefective subretinal drusenoid deposits and hyperreflective  
493 soft drusen across the macula. Hyperreflective foci are present in inner and outer  
494 nuclear layer.

495

## Intraretinal vascular morphologies in treated AMD

### 496 **Figure S4. Initial presentation of left eye, 5 years before death**

497 **A-E.** Near infrared reflectance images (NIR) and radial optical coherence tomography  
498 (OCT) B-scans show non-exudative age-related macular degeneration in the left eye.  
499 Hyporeflective subretinal drusenoid deposits and hyperreflective soft drusen (**B** teal and  
500 fuchsia arrowheads respectively) appear across the macula.

501 **B.** On the recirculation phase of fluorescein angiography (FA), no intraretinal or  
502 subretinal fluid or leakage is present, ensuring absence of active MNV exudation.

503 **F.** A shallow RPE elevation with choroidal hypertransmission (white arrowhead) and  
504 hyperreflective focus was stable on longitudinal follow-up by OCT (**Figure S4**). No  
505 vessel was found in histology. This lesion presumably corresponds to a calcified druse.<sup>39</sup>

506

### 507 **Figure 5. Multimodal imaging, clinical course, and histology of pyramidal type 3** 508 **MNV, OS 4.**

509 **A.** Venous phase fluorescein angiography (FA, **A1**) shows mild leakage at site of type 3  
510 MNV 11 months before death. Green lines on FA represent optical coherence  
511 tomography (OCT) B-scans. Horizontal OCT B-scan (**A2**) displays a hyperreflective  
512 lesion, hyperreflective foci (HRF), and small intraretinal cysts.

513 **B.** Blue lines on near-infrared reflectance (NIR, **B1**), represents histology section in **D**.  
514 Radial OCT B-scan (**B2**) displays enlarged intraretinal cysts, after 5 total injections and 8  
515 weeks following the prior injection. There is also subsidence of the outer plexiform layer  
516 (OPL) and external limiting membrane (ELM).

517 **C.** On radial OCT B-scan (**C2**), intraretinal fluid is reduced after 6 injections and 6 weeks  
518 following the prior injection. Numerous HRF are present in the inner nuclear layer (INL;  
519 **C2**; scale bar 200  $\mu\text{m}$ ).

520 **D.** On histology, type 3 MNV is a pyramidal complex bounded by retinal pigment  
521 epithelium cells. It extends from the INL/ OPL border to basal laminar deposit draping a  
522 calcified druse. Structural damage to Henle's fiber layer at the right of the panel (green  
523 asterisk) may indicate an area of prior intraretinal fluid. Magnified histology is shown in  
524 **Figure 6**. Scale bar 100  $\mu\text{m}$ .

525 Blue line, histology section. Time in months, time before death.

526

## Intraretinal vascular morphologies in treated AMD

### 527 **Figure 6. Pyramidal vascular complex in type 3 MNV, OS 4.**

528 **A, B.** A pyramidal complex includes neovessels ensheathed by thick layers of  
529 collagenous material and flanked by retinal pigment epithelium cells. The complex  
530 extends from the inner nuclear layer (INL) through the outer plexiform layer, Henle fiber  
531 layer, outer nuclear layer (OPL, HFL, ONL, respectively) and terminates at the basal  
532 lamina deposits draping a calcified druse. Bruch's membrane appears intact with no  
533 evidence of a choroidal contribution to the neovessel complex. The external limiting  
534 membrane (ELM) descends at both sides of type 3 MNV base. There is some fluid at the  
535 OPL-HFL border (yellow asterisk in **B**). Areas within dotted green boxes are shown in  
536 **Figure 10.**

537

### 538 **Figure 7. Transmission electron microscopy of pyramidal type 3 MNV, OS 4.**

539 See Figure 8 for light microscopy of OS4. **A.** Neovessel with erythrocyte in the lumen  
540 (blue asterisk) is ensheathed by endothelium, pericyte, and collagenous material (purple,  
541 white, and black asterisks, respectively). Surrounding retinal pigment epithelium (RPE)  
542 cells merge into multi-nucleated cells (red asterisk) or disperse into the Henle fiber layer  
543 (HFL, green asterisk). Phagolysosomes are not visible in the RPE cells.

544 **B-D.** Endothelial cells in the neovessel and comparison vessels are displayed. The  
545 lumen is located at the bottom of all panels.

546 **B.** No fenestrations are detected in the neovessel (orange arrowheads).

547 **C.** Fenestrations are visible in the choriocapillaris (orange arrowheads).

548 **D.** No fenestrations are detected in the deep capillary plexus (orange arrowheads).

549 **E.** Atop the calcified druse (fuchsia asterisk), RPE lipofuscin is more electron-dense at  
550 the druse base than at the druse top (left vs right in the panel). These changes are  
551 consistent with transdifferentiation.

552

### 553 **Figure 8. Multimodal imaging, clinical course, and histology of tangled type 3** 554 **MNV, OD 1.**

555

556 **A.** Green and red lines on near-infrared reflectance (NIR, **A1**) represent optical  
557 coherence tomography (OCT) B-scans corresponding to en face OCT angiography  
558 (OCTA, **A2**) and OCT B-scan with flow signal overlay (**A3**). After 29 total injections and 8  
559 weeks following the prior injection (**A2&A3**), flow signal persists within the tangled  
560 hyperreflective type 3 MNV lesion (green arrowhead). The RPE/Bruch's membrane



## Intraretinal vascular morphologies in treated AMD

561 complex is split by hyporeflective material and appears as a “double layer” sign without  
562 flow signal (**A3**). Red lines in **A2** indicate the segmentation boundaries [outer plexiform  
563 layer (OPL)-retinal pigment epithelium (RPE)] used to create the en face OCTA (**A2**).  
564 **B**. Fluorescein angiography (FA, **B1**) shows late venous phase hyperfluorescence, after  
565 32 total injections and 8 weeks following the last injection. OCT B-scan (**B2**) shows  
566 intraretinal fluid in the inner nuclear and Henle fiber layers surrounding the type 3 MNV  
567 lesion (green arrowhead).  
568 **C**. NIR (**C1**) and radially oriented OCT B-scan (**C2**) shows intraretinal fluid adjacent to  
569 the tangled type 3 MNV lesion (green arrowhead), after 36 total injections and 8 weeks  
570 following the prior injection. Blue line in **C1** represents histology section in panel **D**.  
571 **D**. Panoramic histology shows a horizontally oriented tangled type 3 MNV lesion (green  
572 arrowhead), partly bounded by RPE cells (scale bar 200  $\mu\text{m}$ ). The complex extends from  
573 the inner nuclear layer border to a chipped out calcified druse, which correlates to the  
574 double layer sign in B1. The druse is draped by basal laminar deposit and lacks RPE at  
575 its apex.  
576 Time in months, time before death; BCVA, best corrected visual acuity.

577

578 **Figure 9. Volume rendering of structural optical coherence tomography (OCT,**  
579 **gray) and OCT angiography (OCTA, yellow) of tangled type 3 MNV, OD 1.**

580 **A**. Neovascular blood flow within a hyperreflective structure (white arrowheads) is  
581 observed at the level of the outer nuclear layer (ONL).

582 **B**. Three-dimensional analysis of neovascular blood flow depict an anastomosis above  
583 the retinal pigment epithelium (RPE)/ Bruch’s membrane (BrM; green section) and a  
584 tangled structure connecting to the superficial artery (red arrow) and vein (blue arrow).

585 **C**. Volume rendering of OCTA with orthogonal structural sections evidence a tangled  
586 neovascular lesion.

587

588 **Figure S10. Tangled vascular complex in type 3 MNV, OD 1.**

589 **A-C**. Tangled vascular complex (fuchsia arrowheads indicate lumen) spans 249  $\mu\text{m}$   
590 horizontally towards the superior perifovea (**A**, 759  $\mu\text{m}$  from fovea; **B**, 719  $\mu\text{m}$  from fovea;  
591 **C**, 552  $\mu\text{m}$  from fovea). The complex is partly ensheathed by collagenous material and is  
592 flanked by retinal pigment epithelium (RPE) cells. Two cells rest entirely within the outer  
593 plexiform layer (OPL)/ inner nuclear layer (INL; light blue arrowhead in **A**). The INL/OPL  
594 subsides, and the vascular complex extends from the INL/OPL border through the Henle

## Intraretinal vascular morphologies in treated AMD

595 fiber layer (HFL)/ outer nuclear layer (ONL). The complex adheres to basal laminar  
596 deposits (BLamD) draping a calcified druse (d). Bruch's membrane (BrM) appears intact  
597 without evidence of a choroidal contribution. The external limiting membrane (ELM)  
598 descends at both edges of the calcified druse (yellow arrowheads in **B**). Vessel walls do  
599 not exhibit obvious arterial or venous features. Vessel diameter within the INL was larger  
600 than 15  $\mu\text{m}$ , suggesting drainage venules.

601

### 602 **Figure 11. Deep retinal age-related microvascular anomaly (DRAMA), OS1.**

603 **A.** Near infrared reflectance (NIR) shows drusen and subretinal drusenoid deposits 11  
604 months before death. Blue line, plane of histology section.

605 **B.** Fluorescein angiography (FA) recirculation phase shows minimal leakage at the site  
606 of DRAMA.

607 **C.** On histology, a vessel extends downwards (yellow arrowheads) from the inner  
608 nuclear layer (INL) into the outer plexiform layer (OPL) above a druse.

609

### 610 **Figure 12. Multimodal imaging and histology of deep retinal age-related** 611 **microvascular anomaly (DRAMA) with intraretinal RPE complex, OS 3.**

612  
613 **A.** Fluorescein angiography (FA) venous phase shows faint staining, 11 months before  
614 death (**A1**). Optical coherence tomography (OCT, **A2**) shows a stack of intraretinal  
615 hyperreflective foci (HRF, fuchsia arrowhead). No intraretinal cysts are visible.

616 **B.** After 6 total injections and 6 weeks following the prior injection, the stacked lesion  
617 (fuchsia arrowhead) is stable, without cysts. A plume of HRF extend nasally 2 months  
618 before death. Green lines, OCT B-scans; blue line, histology section.

619 **C.** On histology, a retinal pigment epithelium tower (fuchsia arrowhead) rises upward  
620 from a soft druse. Cells surround a vessel and extend into the outer plexiform layer.  
621 Magnified histology is shown in [Figure 13](#).

622

### 623 **Figure 13. RPE complex associated with deep retinal age-related microvascular** 624 **anomaly (DRAMA), OS 3.**

625 **A.** A "hand" shaped complex consisting of retinal pigment epithelium (RPE) cells  
626 surrounds vessel extending downward from the deep capillary plexus. Electron  
627 microscopy of the area in the dotted fuchsia box is shown in [Figure S14](#).

## Intraretinal vascular morphologies in treated AMD

628 **B.** The RPE complex extends upward to the inner nuclear layer (INL). On either side of  
629 this complex, there is no subsidence of outer plexiform layer (OPL) or external limiting  
630 membrane (ELM), and the outer nuclear layer (ONL) is thinned. The complex emanates  
631 from a continuous RPE layer over basal laminar deposit (BLamD) and a soft druse. The  
632 druse is artifactually detached from Bruch's membrane (BrM).

633 **C-E.** Endothelial cell (EC) ultrastructure in DRAMA and comparison vessels are shown.  
634 Vascular lumen is at the bottom of all panels.

635 **C.** No fenestrations are visible in the DRAMA (red blood cell, RBC).

636 **D.** No fenestrations are visible in the deep capillary plexus (pericyte, P).

637 **E.** Fenestrations are visible in the choriocapillaris endothelium (orange arrowheads;  
638 white blood cell, WBC).

639

640 **Figure S14. Transmission electron microscopy of DRAMA with RPE complex, OS**

641 **3.**

642 The Vessel is ensheathed by an endothelial (E) cell and a pericyte (P), with little  
643 collagen. The Lumen contains a leukocyte (LC) and a red blood cell (RBC). The  
644 surrounding tower of retinal pigment epithelium (RPE) is multicellular (white asterisk),  
645 and multinucleated (fuchsia asterisks). RPE organelle packing density and electron-  
646 density is similar to in-layer RPE cells (not shown).

647

648 **Figure 15. Multimodal imaging of deep retinal age-related microvascular**  
649 **anomalies (DRAMAs), OD 3.**

650 **A.** Fluorescein angiography (FA) venous phase shows mild hyperfluorescence 11  
651 months before death. **B.** Green and blue lines on near-infrared reflectance (NIR),  
652 represent optical coherence tomography (OCT) B-scan (C) and histology section (D). **C.**  
653 Horizontally oriented OCT B-scan with OCT angiography (OCTA) flow overlay shows  
654 cyst-like spaces in the Henle fiber layer adjacent to a pair of hyperreflective DRAMAs  
655 (fuchsia arrowheads). The retinal pigment epithelium/Bruch's membrane complex to the  
656 left is split by hyporefective material. **D.** OCTA shows a pair of intraretinal flow signals  
657 (fuchsia arrowheads). **E.** Histology shows a pair of vessels extending from the inner  
658 nuclear layer border to the outer nuclear layer. Magnified histology is shown in **Figure**  
659 **16.**

660

## Intraretinal vascular morphologies in treated AMD

661 **Figure 16. Vascular complex of deep retinal age-related microvascular anomaly**  
662 **(DRAMA), OD 3.**

663  
664 **A, B.** A penetrating pair of vessels, (DRAMAs, fuchsia arrowheads) ensheathed by  
665 collagenous material dives from the inner nuclear layer (INL) into the Henle fiber layer  
666 (HFL)/outer nuclear layer (ONL). Next to the vessels is a degenerative cyst in the Henle  
667 fiber layer (HFL). There is no subsidence of external limiting membrane (ELM). The ONL  
668 is thinned.

669 **B.** Retinal pigment epithelium (RPE) from the edge of a druse (d) migrates towards the  
670 lower edge of the vessel complex, right side.

671

672

673 **Video S1.**

674 **Volume rendering of structural OCT (gray) and OCTA (yellow) of tangled type 3**

675 **MNV, OD 1.**

676 The cube is rotated 180° to highlight vascular findings in the superior macula region.

677 Coronal view demonstrates blood flow immediately below the deep capillary plexus level

678 in two separate areas. Superposition with structural OCT (gray channel) demonstrates

679 neovascular blood flow within an hyperreflective structure at the outer nuclear layer and

680 above Bruch's membrane (BrM). The superficial arteries (red) and veins (blue) in the

681 vicinity of the lesion are outlined after fluorescein angiography analysis. Three-

682 dimensional analysis of neovascular blood flow depicts an anastomosis right above BrM

683 (green section) Spinning around the neovascular blood-flow highlights separate inflow

684 and outflow.

## Intraretinal vascular morphologies in treated AMD

### References

1. Freund KB, Zweifel SA, Engelbert M. Do we need a new classification for choroidal neovascularization in age-related macular degeneration? *Retina*. 2010;30(9):1333-49.
2. Su D, Lin S, Phasukkijwatana N, et al. An updated staging system of type 3 neovascularization using spectral domain optical coherence tomography. *Retina* 2016;36:S40-S9.
3. Berlin A, Cabral D, Chen L, et al. Correlation of Optical Coherence Tomography Angiography of Type 3 Macular Neovascularization With Corresponding Histology. *JAMA Ophthalmol*. 2022;140(6):628-633.
4. Spaide RF, Jaffe GJ, Sarraf D, et al. Consensus nomenclature for reporting neovascular age-related macular degeneration data: consensus on neovascular age-related macular degeneration nomenclature study group. *Ophthalmology* 2020;127(5):616-36.
5. Yannuzzi LA, Negrão S, Tomohiro I, et al. Retinal angiomatous proliferation in age-related macular degeneration. *Retina* 2012;32:416-34.
6. Jung JJ, Chen CY, Mrejen S, et al. The incidence of neovascular subtypes in newly diagnosed neovascular age-related macular degeneration. *American Journal of Ophthalmology* 2014;158(4):769-79. e2.
7. Kim JH, Kim JW, Kim CG, Lee DW. Influence of fellow-eye examination interval on visual acuity at fellow-eye neovascularization in unilateral type 3 neovascularization. *Retina* 2020;40(7):1255-61.
8. Kwak JH, Park WK, Kim RY, et al. Unaffected fellow eye neovascularization in patients with type 3 neovascularization: Incidence and risk factors. *PLoS One* 2021;16(7):e0254186.
9. Sacconi R, Forte P, Capuano V, et al. OCT-A characterization of evolving lesions in fellow eyes of exudative type 3 MNV patients. *Retina* 2022;10.1097.
10. Freund KB, Ho I-V, Barbazetto IA, et al. Type 3 neovascularization: the expanded spectrum of retinal angiomatous proliferation. *Retina* 2008;28(2):201-11.
11. Najeeb BH, Deak G, Schmidt-Erfurth U, Gerendas BS. The RAP study, report two: the regional distribution of macular neovascularization type 3, a novel insight into its etiology. *Retina* 2020;40(12):2255-62.
12. Haj Najeeb B, Deak GG, Sacu S, et al. The RAP study, report 4: morphological and topographical characteristics of multifocal macular neovascularization type 3. *Graefes Archive for Clinical and Experimental Ophthalmology* 2022;260(1):141-7.
13. Haj Najeeb B, Deak GG, Schmidt-Erfurth U, Gerendas BS. The RAP study, report 3: Discoloration of the macular region in patients with macular neovascularization type 3. *Acta Ophthalmologica* 2021.
14. Borrelli E, Sacconi R, Klose G, et al. Rotational three-dimensional OCTA: a notable new imaging tool to characterize type 3 macular neovascularization. *Scientific Reports* 2019;9(1):1-8.
15. Shimada H, Kawamura A, Mori R, Yuzawa M. Clinicopathological findings of retinal angiomatous proliferation. *Graefes Archive for Clinical and Experimental Ophthalmology* 2007;245(2):295-300.
16. Li M, Dolz-Marco R, Messinger JD, et al. Clinicopathologic Correlation of Anti-Vascular Endothelial Growth Factor-Treated Type 3 Neovascularization in Age-Related Macular Degeneration. *Ophthalmology* 2018;125(2):276-87.
17. Sacconi R, Freund KB, Yannuzzi LA, et al. The expanded spectrum of perifoveal exudative vascular anomalous complex. *American Journal of Ophthalmology* 2017;184:137-46.
18. Gilani F, Gal-Or O, Freund KB. Spontaneous rupture and involution of a “macro-microaneurysm” in diabetic retinopathy. *Retina* 2017;37(6):e73-e4.
19. Spaide RF, Barquet LA. Retinal capillary macroaneurysms. *Retina* 2019;39(10):1889-95.
20. Sacconi R, Cohen SY, Borrelli E, et al. Correspondence. *Retina* 2019;39(11):e48-e9.

## Intraretinal vascular morphologies in treated AMD

21. Spaide RF. Correspondence Reply. *Retina* 2019;39(11):E49-E50.
22. Sacconi R, Borrelli E, Sadda S, et al. Nonexudative perifoveal vascular anomalous complex: the subclinical stage of perifoveal exudative vascular anomalous complex? *American Journal of Ophthalmology* 2020;218:59-67.
23. Querques G, Kuhn D, Massamba N, et al. Perifoveal exudative vascular anomalous complex. *Journal Français d'Ophthalmologie* 2011;34(8):559. e1-. e4.
24. Cabral D, Ramtohul P, Fradinho A, Freund KB. Volume Rendering of Deep Retinal Age-Related Microvascular Anomalies. *Ophthalmol Retina* 2022.
25. Chen L, Messinger JD, Sloan KR, et al. Nonexudative macular neovascularization supporting outer retina in age-related macular degeneration: a clinicopathologic correlation. *Ophthalmology* 2020;127(7):931-47.
26. Querques G, Querques L, Forte R, et al. Precursors of type 3 neovascularization: a multimodal imaging analysis. *Retina* 2013;33(6):1241-8.
27. Association WM. World Medical Association Declaration of Helsinki: ethical principles for medical research involving human subjects. *JAMA* 2013;310(20):2191-4.
28. Edemekong P, Annamaraju P, Haydel M. Health Insurance Portability and Accountability Act. StatPearls Treasure Island (FL): StatPearls Publishing 2021.
29. Rocholz R, Teussink M, Dolz-Marco R, et al. SPECTRALIS optical coherence tomography angiography (OCTA): principles and clinical applications. *Heidelb Eng Acad* 2018(September):1-10.
30. Cabral D, Fradinho AC, Pereira T, et al. Macular Vascular Imaging and Connectivity Analysis Using High-Resolution Optical Coherence Tomography. *Translational Vision Science & Technology* 2022;11(6):2-.
31. Breazzano MP, Bacci T, Curcio CA, Freund KB. Novel multimodal imaging and volume rendering of type 3 macular neovascularization. *Retina* 2020;40(10):e55-e7.
32. Xu X, Yannuzzi NA, Fernández-Avellaneda P, et al. Differentiating veins from arteries on optical coherence tomography angiography by identifying deep capillary plexus vortices. *American Journal of Ophthalmology* 2019;207:363-72.
33. Kim JH, Chang YS, Kim JW, et al. Characteristics of type 3 neovascularization lesions: focus on the incidence of multifocal lesions and the distribution of lesion location. *Retina* 2020;40(6):1124-31.
34. Group ETDRSR. Grading diabetic retinopathy from stereoscopic color fundus photographs—an extension of the modified Airlie House classification: ETDRS report number 10. *Ophthalmology* 1991;98(5):786-806.
35. Pongsachareonnont P, Somkijrungraj T, Assavapongpaiboon B, et al. Foveal and parafoveal choroidal thickness pattern measuring by swept source optical coherence tomography. *Eye* 2019;33(9):1443-51.
36. Balaratnasingam C, An D, Sakurada Y, et al. Comparisons between histology and optical coherence tomography angiography of the periarterial capillary-free zone. *American Journal of Ophthalmology* 2018;189:55-64.
37. Litts KM, Messinger JD, Dellatorre K, et al. Clinicopathological correlation of outer retinal tubulation in age-related macular degeneration. *JAMA Ophthalmology* 2015;133(5):609-12.
38. Balaratnasingam C, An D, Freund KB, et al. Correlation between histologic and OCT angiography analysis of macular circulation. *Ophthalmology* 2019;126(11):1588-9.
39. Berlin A MJ, Ferrara D, Freund KB, Curcio CA. OCT features relevant to neovascular AMD management and non-neovascular AMD progression: clinicopathologic correlation. *Retinal Cases and Brief Reports* 2022 ; 9900:10.1097.
40. Berlin A, Chen L, Messinger J, et al. Double-layer sign in neovascular age-related macular degeneration—do we treat? *Acta Ophthalmologica* 2022;100(3):348-9.
41. Snodderly DM, Weinhaus RS, Choi J. Neural-vascular relationships in central retina of macaque monkeys (*Macaca fascicularis*). *Journal of Neuroscience* 1992;12(4):1169-93.
42. Balaratnasingam C, Messinger JD, Sloan KR, et al. Histologic and optical coherence tomographic correlates in drusenoid pigment epithelium detachment in age-related macular degeneration. *Ophthalmology* 2017;124(5):644-56.

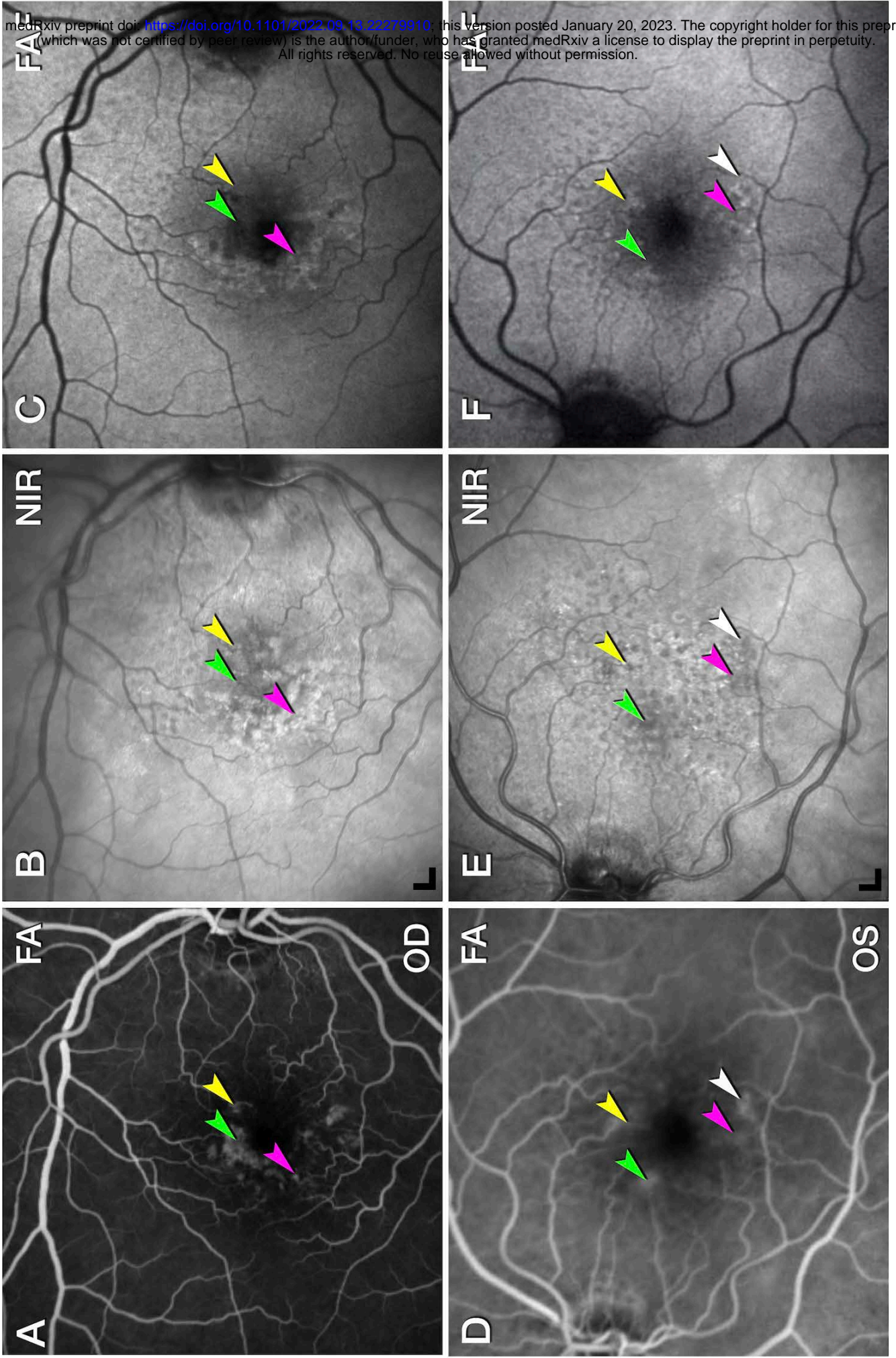
### Intraretinal vascular morphologies in treated AMD

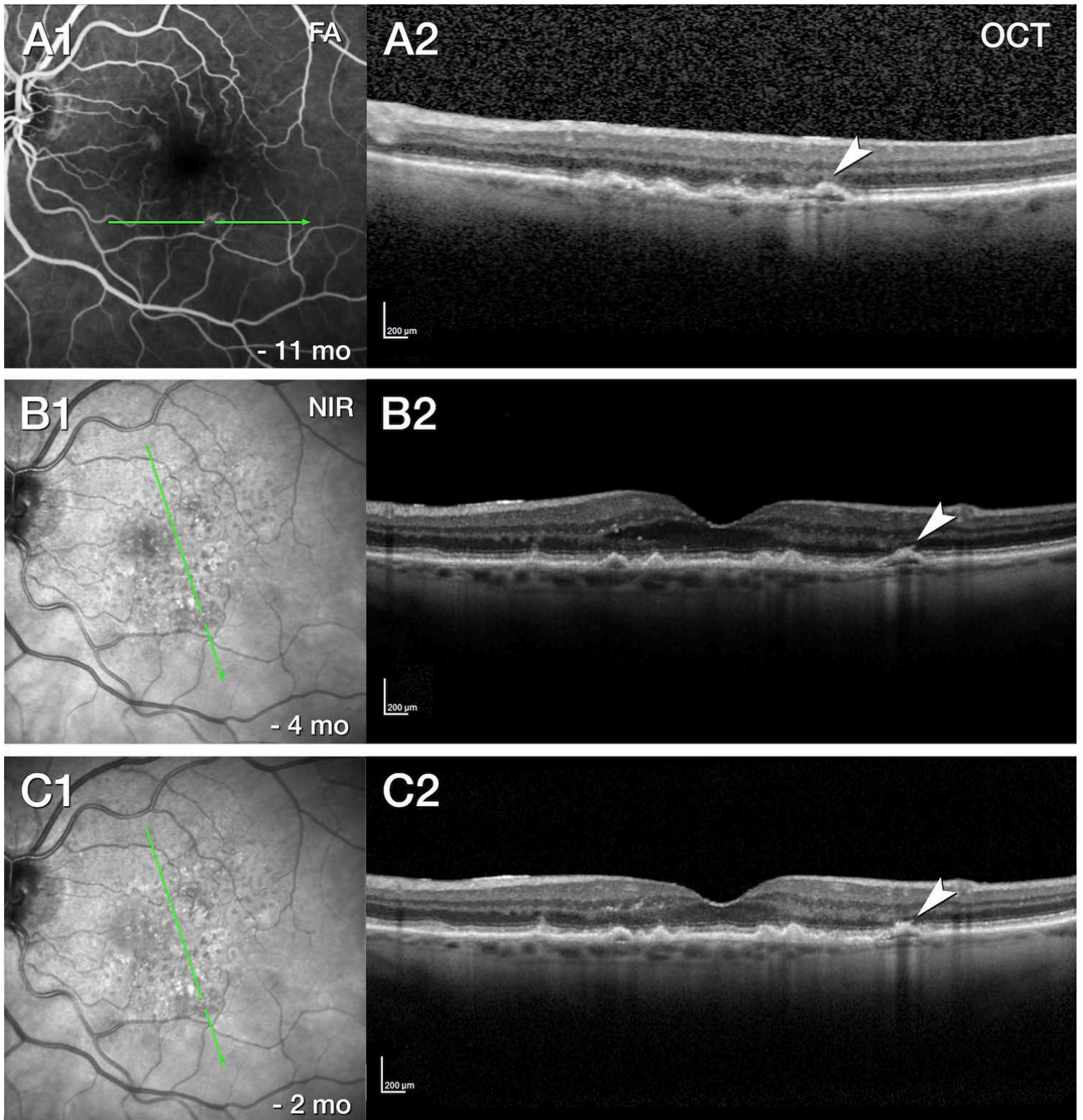
43. Cao D, Leong B, Messinger JD, et al. Hyperreflective foci, optical coherence tomography progression indicators in age-related macular degeneration, include transdifferentiated retinal pigment epithelium. *Investigative Ophthalmology & Visual Science* 2021;62(10):34-.
44. Najeeb BH, Deak GG, Mylonas G, et al. The RAP study, report 5: rediscovering macular neovascularization Type 3: multimodal imaging of fellow eyes over 24 months. *Retina* 2022;42(3):485.
45. Najeeb BH, Deak GG, Schmidt-Erfurth UM, Gerendas BS. RAP study, report 1: novel subtype of macular neovascularisation type III, cilioretinal MNV3. *British Journal of Ophthalmology* 2021;105(1):113-7.
46. Querques G, Souied EH, Freund KB. How has high-resolution multimodal imaging refined our understanding of the vasogenic process in type 3 neovascularization? *Retina* 2015; 35(4):603-13.
47. Borrelli E, Souied EH, Freund KB, et al. Reduced choriocapillaris flow in eyes with type 3 neovascularization and age-related macular degeneration. *Retina* 2018;38(10):1968-76.
48. Koizumi H, Iida T, Saito M, et al. Choroidal circulatory disturbances associated with retinal angiomas proliferation on indocyanine green angiography. *Graefes Archive for Clinical and Experimental Ophthalmology* 2008;246(4):515-20.
49. Caramoy A, Ristau T, Lechanteur YT, et al. Environmental and genetic risk factors for retinal angiomas proliferation. *Acta Ophthalmologica* 2014;92(8):745-8.
50. Daniel E, Shaffer J, Ying G-s, et al. Outcomes in eyes with retinal angiomas proliferation in the comparison of age-related macular degeneration treatments trials (CATT). *Ophthalmology* 2016;123(3):609-16.
51. Spaide RF. Fundus autofluorescence and age-related macular degeneration. *Ophthalmology* 2003;110(2):392-9.
52. Yannuzzi LA, Freund KB, Takahashi BS. Review of retinal angiomas proliferation or type 3 neovascularization. *Retina*. 2008; 28(3):375-84
53. Cho HJ, Lim SH, Kim J, et al. Assessing the long-term evolution of type 3 neovascularization in age-related macular degeneration using optical coherence tomography angiography. *Graefes Archive for Clinical and Experimental Ophthalmology* 2021:1-9.
54. Kim JH, Chang YS, Kim JW, et al. Difference in treatment outcomes according to optical coherence tomography-based stages in type 3 neovascularization (retinal angiomas proliferation). *Retina* 2018;38(12):2356-62.
55. Sacconi R, Battista M, Borrelli E, et al. OCT-A characterisation of recurrent type 3 macular neovascularisation. *British Journal of Ophthalmology* 2021;105(2):222-6.
56. Huang D, Jia Y, Rispoli M, et al. OCT angiography of time course of choroidal neovascularization in response to anti-angiogenic treatment. *Retina* 2015;35(11):2260.
57. Skalet AH, Miller AK, Klein ML, et al. Clinicopathologic correlation of retinal angiomas proliferation treated with ranibizumab. *Retina* 2017;37(8):1620.
58. Han JW, Cho HJ, Kang DH, et al. Changes in optical coherence tomography angiography and disease activity in type 3 neovascularization after anti-vascular endothelial growth factor treatment. *Retina* 2020;40(7):1245-54.
59. Tolentino MJ, Miller JW, Gragoudas ES, et al. Intravitreal injections of vascular endothelial growth factor produce retinal ischemia and microangiopathy in an adult primate. *Ophthalmology* 1996;103(11):1820-8.
60. Tolentino MJ, McLeod DS, Taomoto M, et al. Pathologic features of vascular endothelial growth factor-induced retinopathy in the nonhuman primate. *American Journal of Ophthalmology* 2002;133(3):373-85.
61. Jackson TL, Danis RP, Goldbaum M, et al. Retinal vascular abnormalities in neovascular age-related macular degeneration. *Retina* 2014;34(3):568-75.
62. Spaide RF. New proposal for the pathophysiology of type 3 neovascularization as based on multimodal imaging findings. *Retina* 2019;39(8):1451-64.

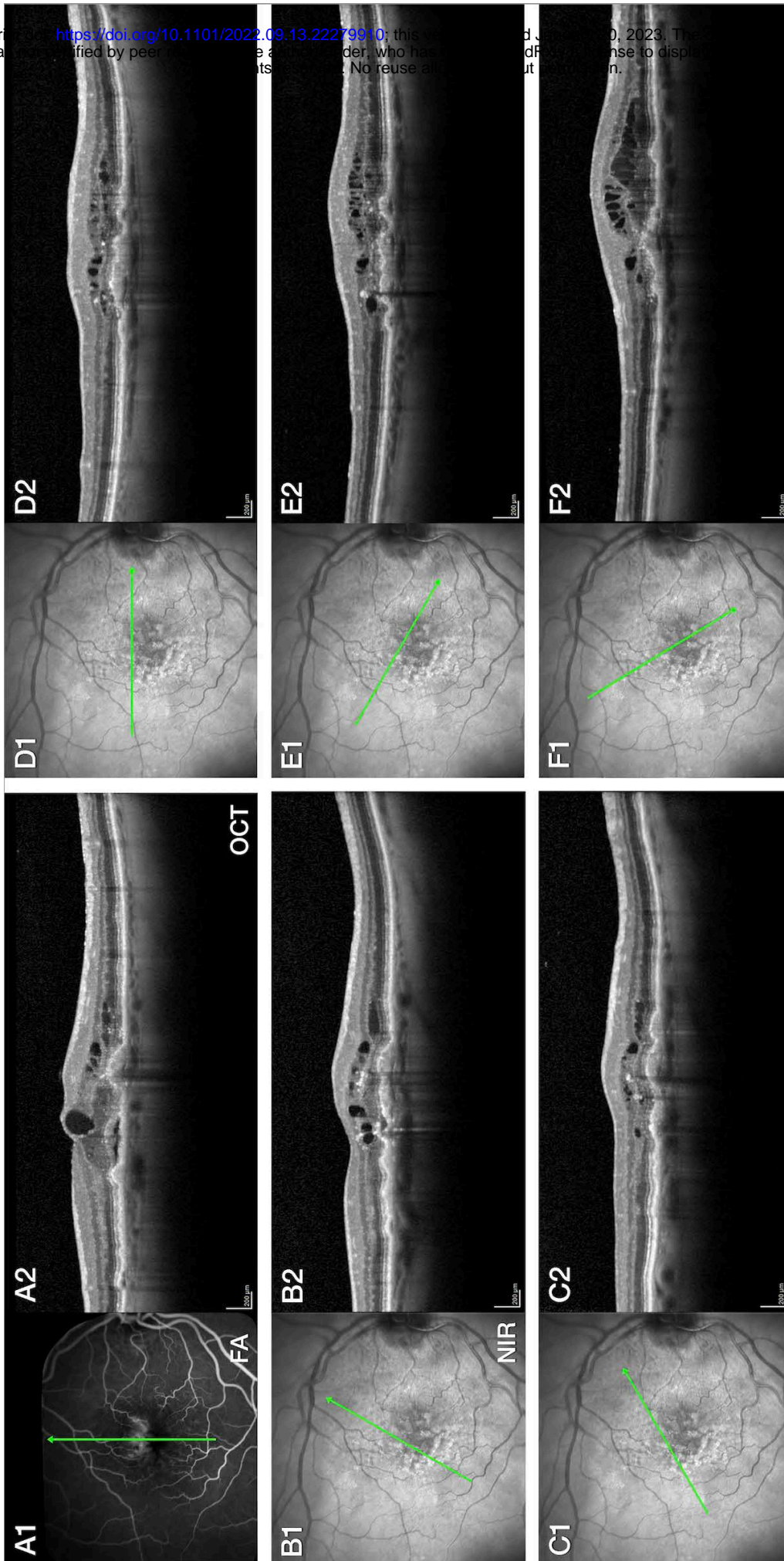
### Intraretinal vascular morphologies in treated AMD

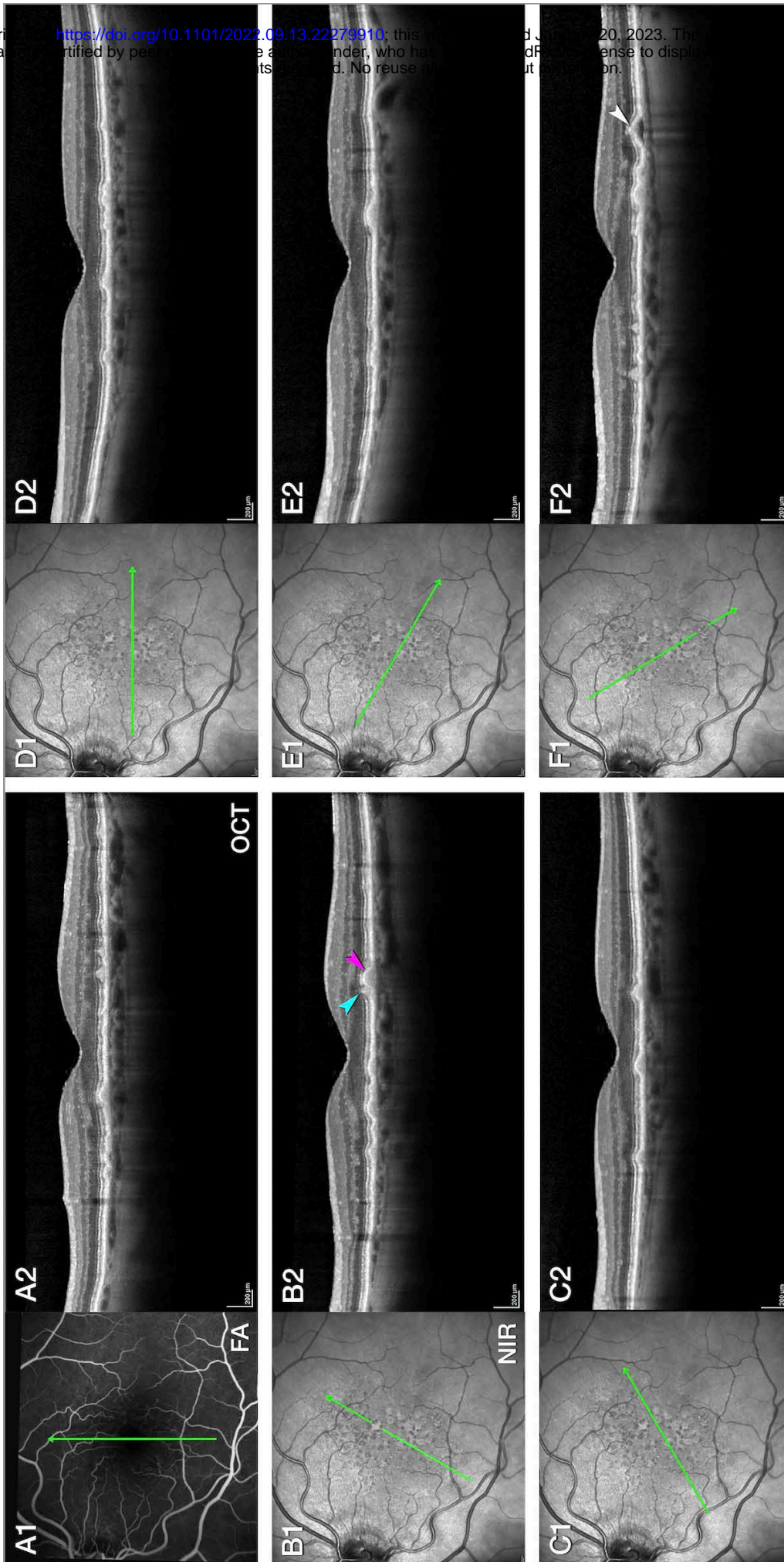
63. Hayreh SS. Segmental nature of the choroidal vasculature. *British Journal of Ophthalmology* 1975;59(11):631-48.
64. Hayreh SS. In vivo choroidal circulation and its watershed zones. *Eye* 1990;4(2):273-89.
65. Hayreh SS. Posterior ciliary artery circulation in health and disease the Weisenfeld lecture. *Investigative Ophthalmology & Visual Science* 2004;45(3):749-57.
66. Yamazaki T, Koizumi H, Yamagishi T, Kinoshita S. Subfoveal choroidal thickness in retinal angiomatous proliferation. *Retina* 2014;34(7):1316-22.
67. Kim JH, Kim JR, Kang SW, et al. Thinner choroid and greater drusen extent in retinal angiomatous proliferation than in typical exudative age-related macular degeneration. *American Journal of Ophthalmology* 2013;155(4):743-9. e2.
68. Tan R, Guymer RH, Luu CD. Subretinal drusenoid deposits and the loss of rod function in intermediate age-related macular degeneration. *Investigative Ophthalmology & Visual Science* 2018;59(10):4154-61.
69. Tan RS, Guymer RH, Aung K-Z, et al. Longitudinal assessment of rod function in intermediate age-related macular degeneration with and without reticular pseudodrusen. *Investigative Ophthalmology & Visual Science* 2019;60(5):1511-8.
70. Chen KG, Alvarez JA, Yazdanie M, et al. Longitudinal study of dark adaptation as a functional outcome measure for age-related macular degeneration. *Ophthalmology* 2019;126(6):856-65.
71. Zhang Y, Sadda SR, Sarraf D, et al. Spatial Dissociation of Subretinal Drusenoid Deposits and Impaired Scotopic and Mesopic Sensitivity in AMD. *Investigative Ophthalmology & Visual Science* 2022;63(2):32-.
72. Nigalye AK, Hess K, Pundlik SJ, et al. Dark Adaptation and Its Role in Age-Related Macular Degeneration. *Journal of Clinical Medicine* 2022;11(5):1358.
73. Zheng F, Zhang Q, Shi Y, et al. Age-dependent changes in the macular choriocapillaris of normal eyes imaged with swept-source optical coherence tomography angiography. *American Journal of Ophthalmology* 2019;200:110-22.
74. Ingram NT, Fain GL, Sampath AP. Elevated energy requirement of cone photoreceptors. *Proceedings of the National Academy of Sciences* 2020;117(32):19599-603.
75. Borrelli E, Mastropasqua L, Souied E, et al. Longitudinal assessment of type 3 macular neovascularization using three-dimensional volume-rendering optical coherence tomography angiography. *Canadian Journal of Ophthalmology* 2021.

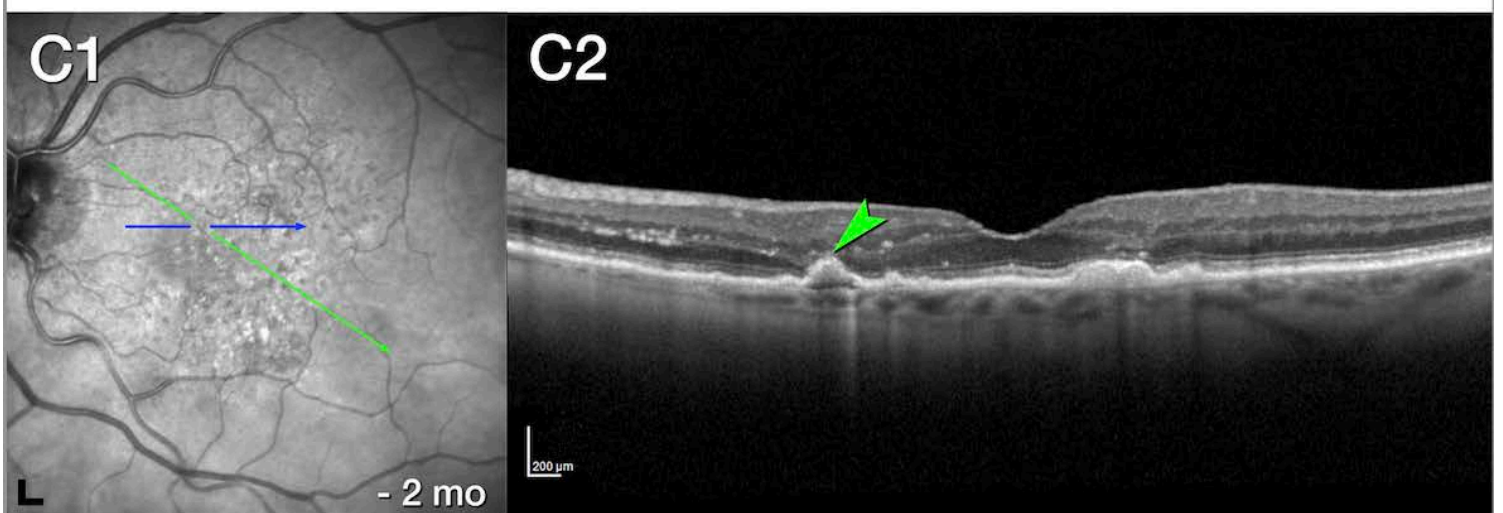
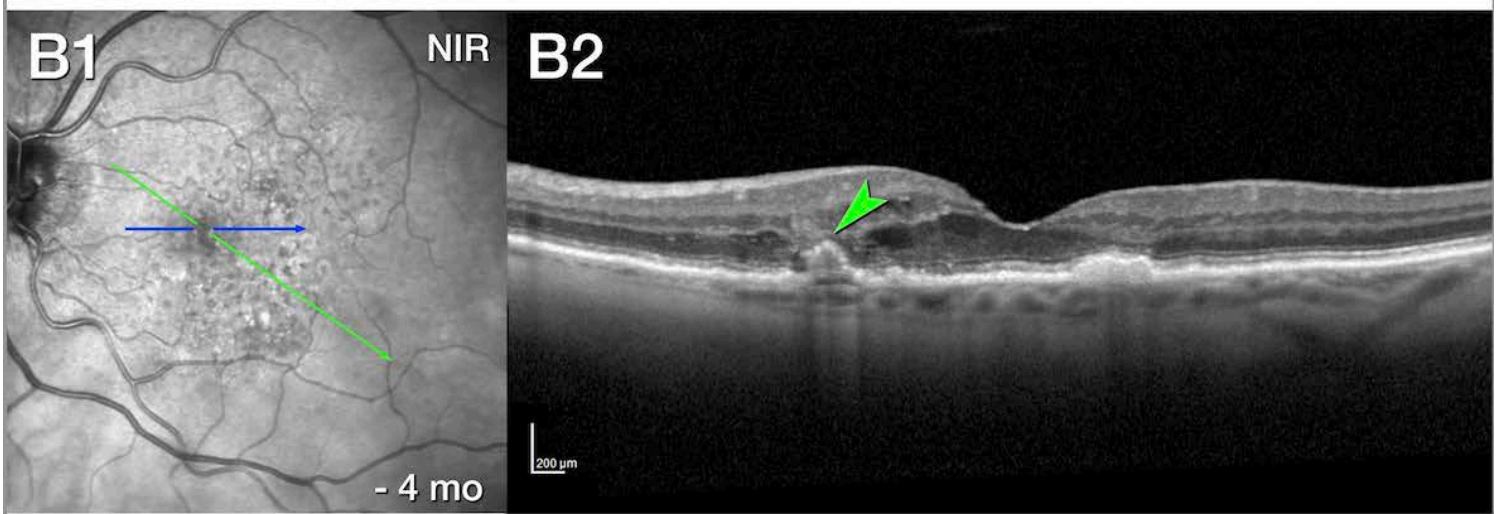
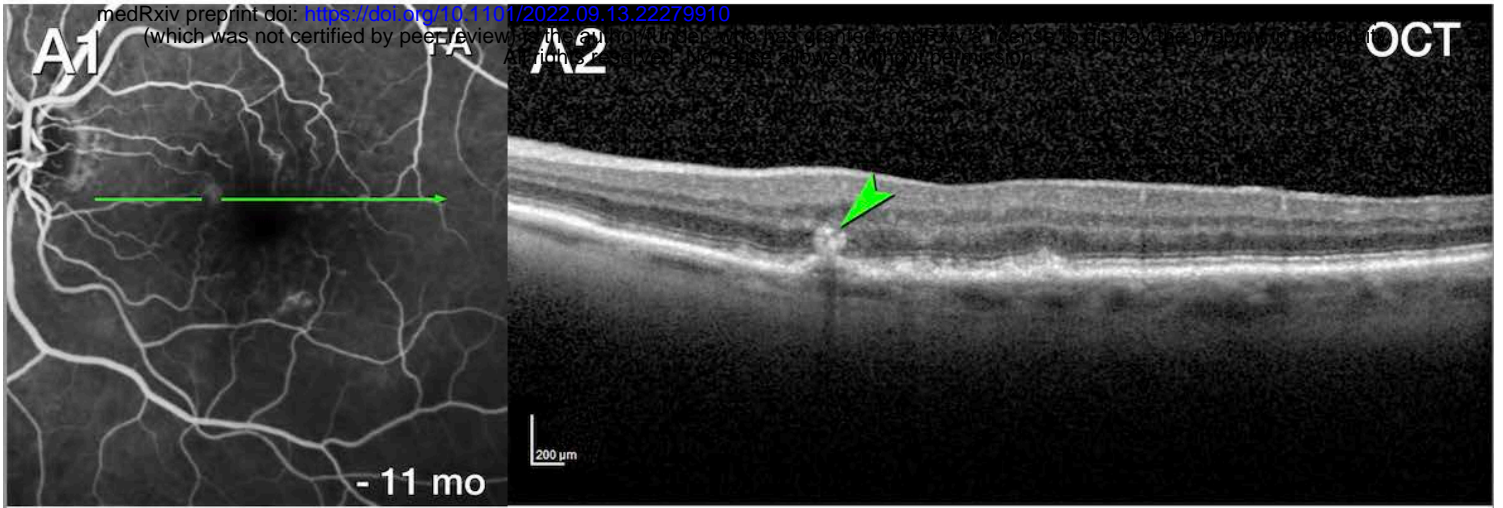


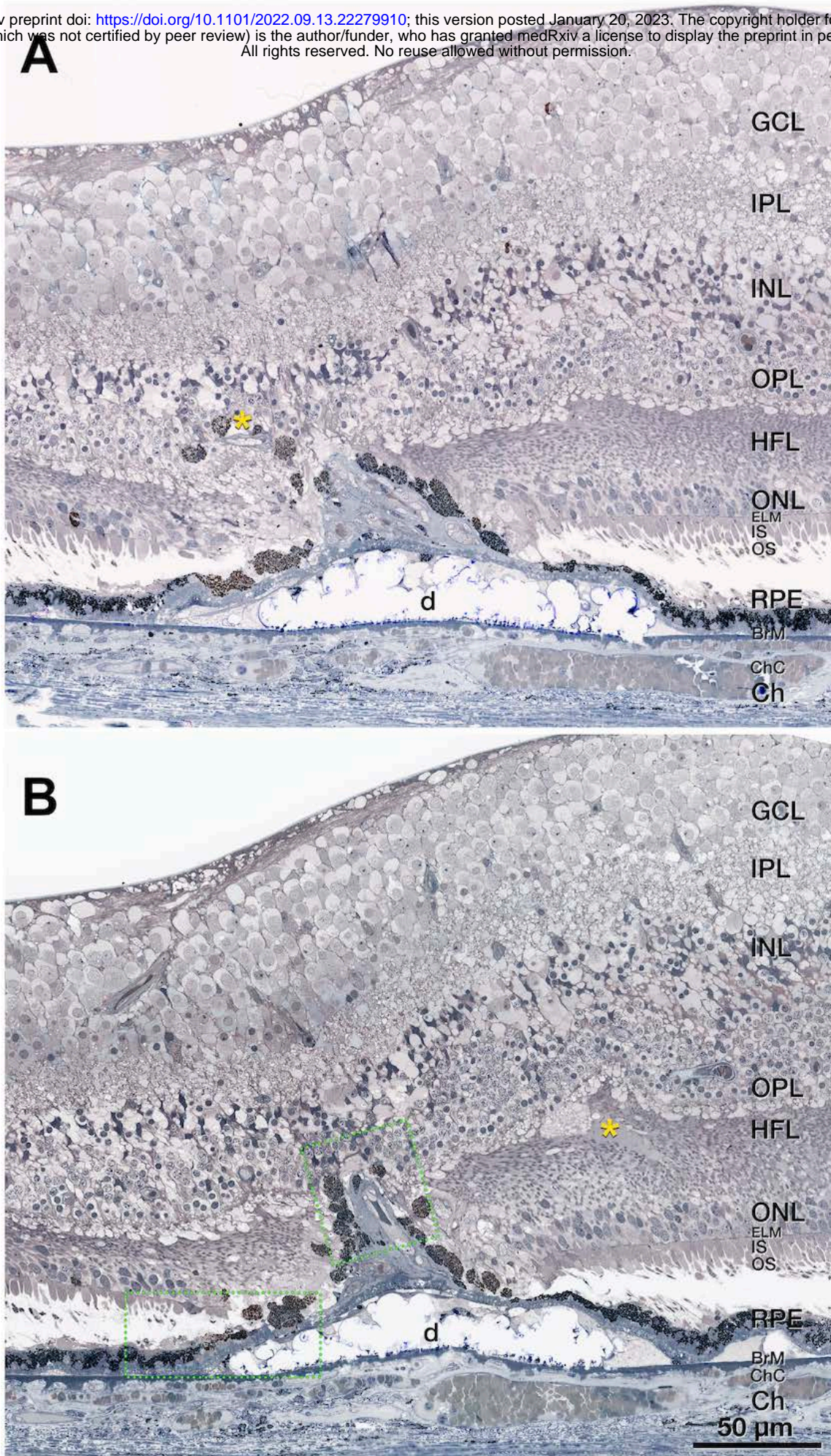


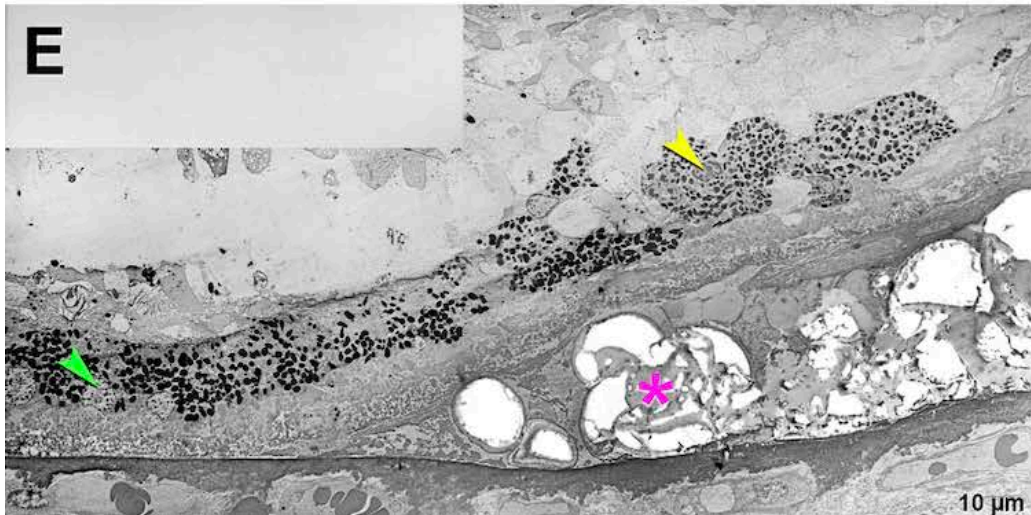
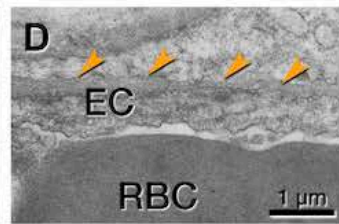
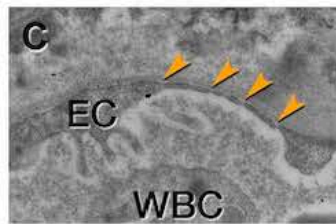
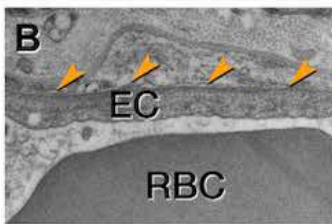
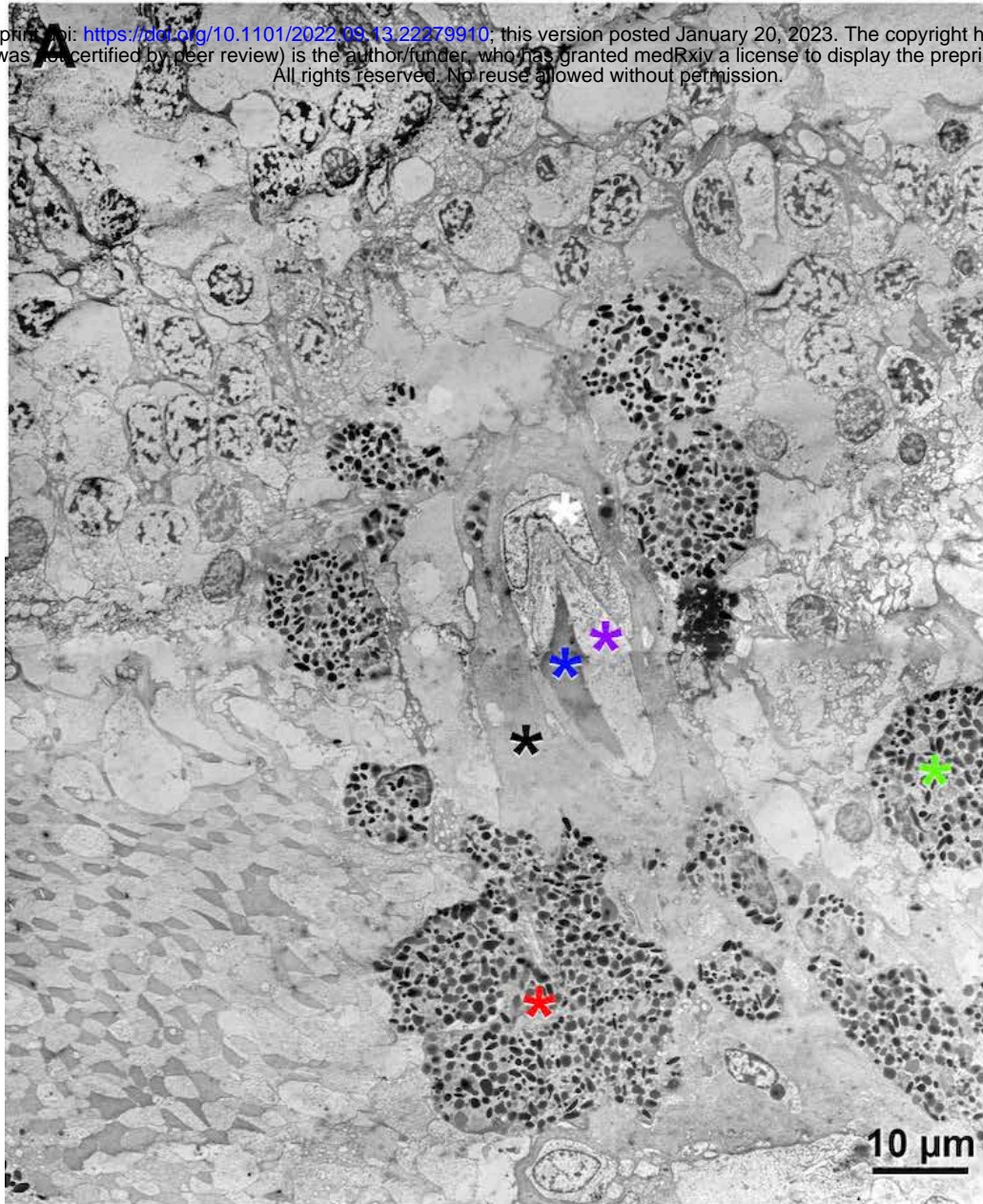


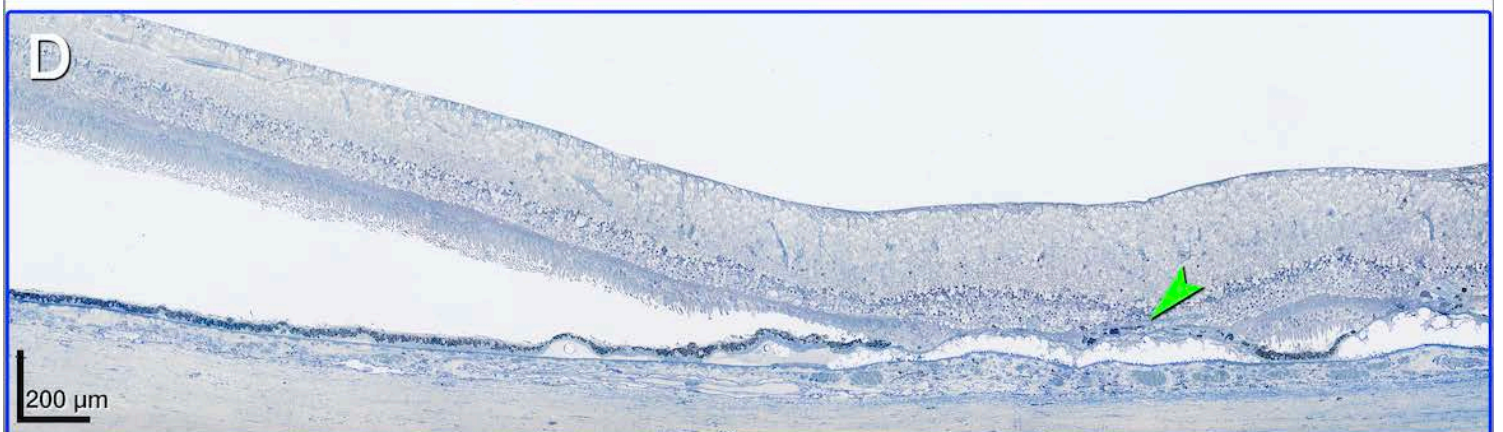
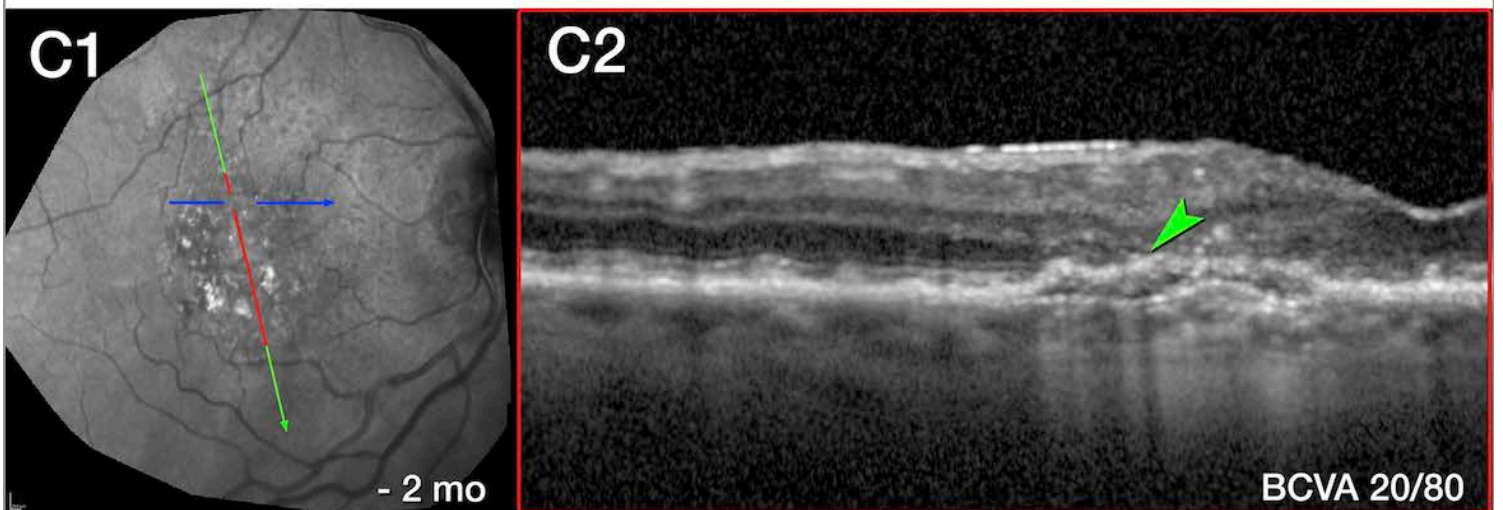
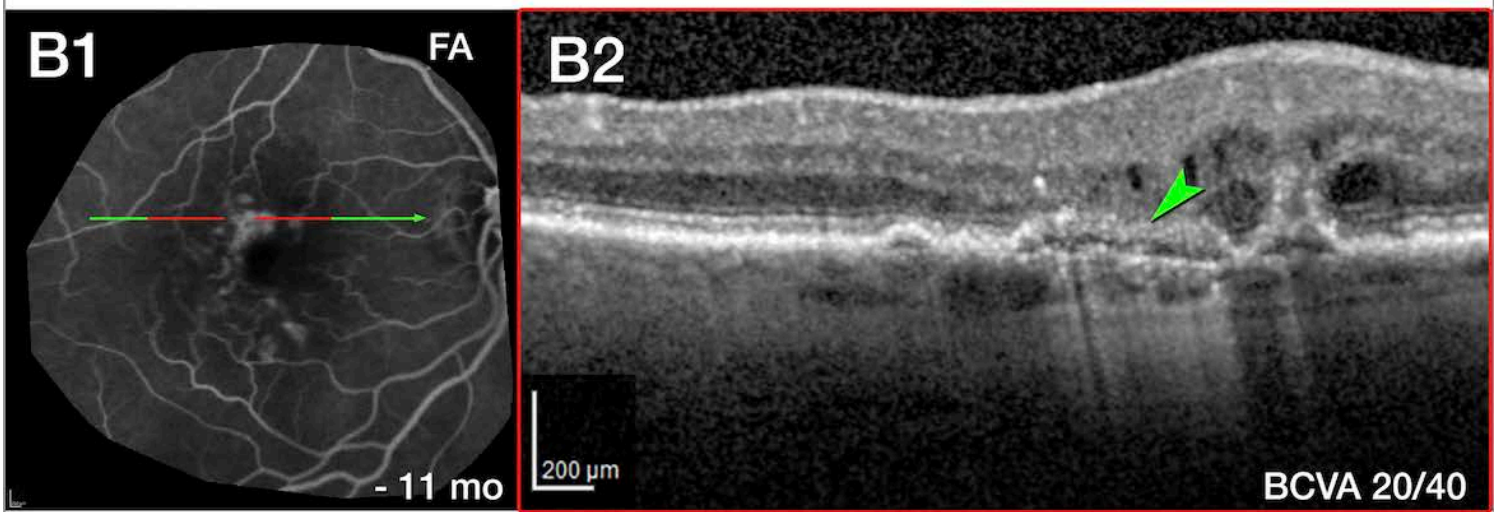
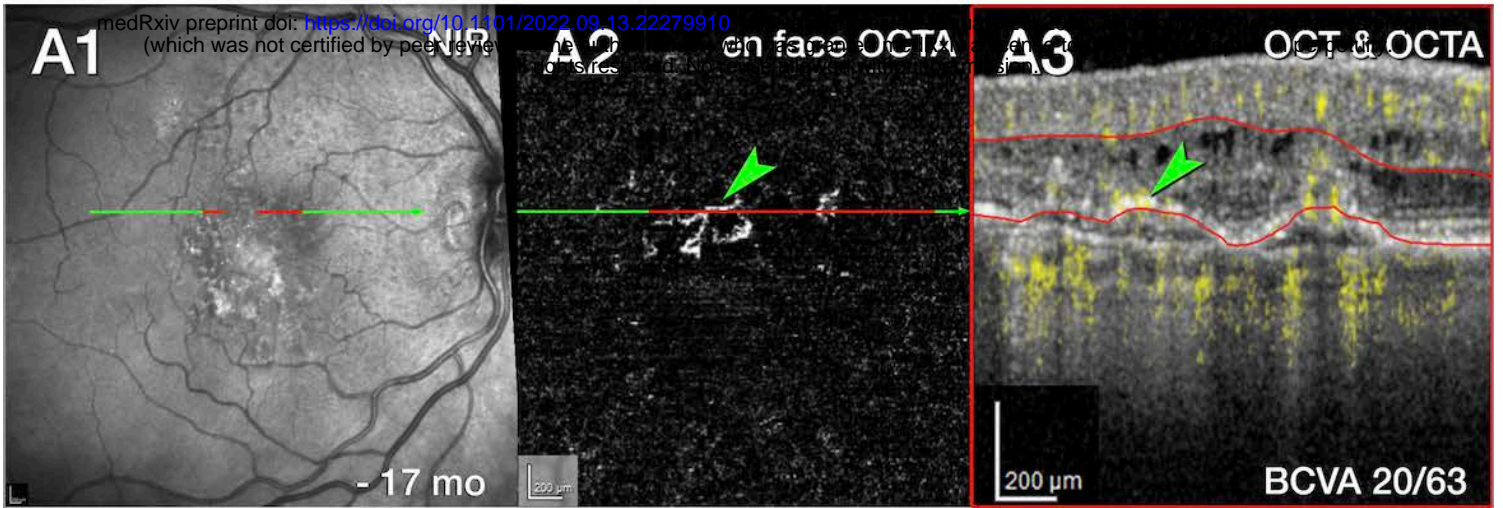




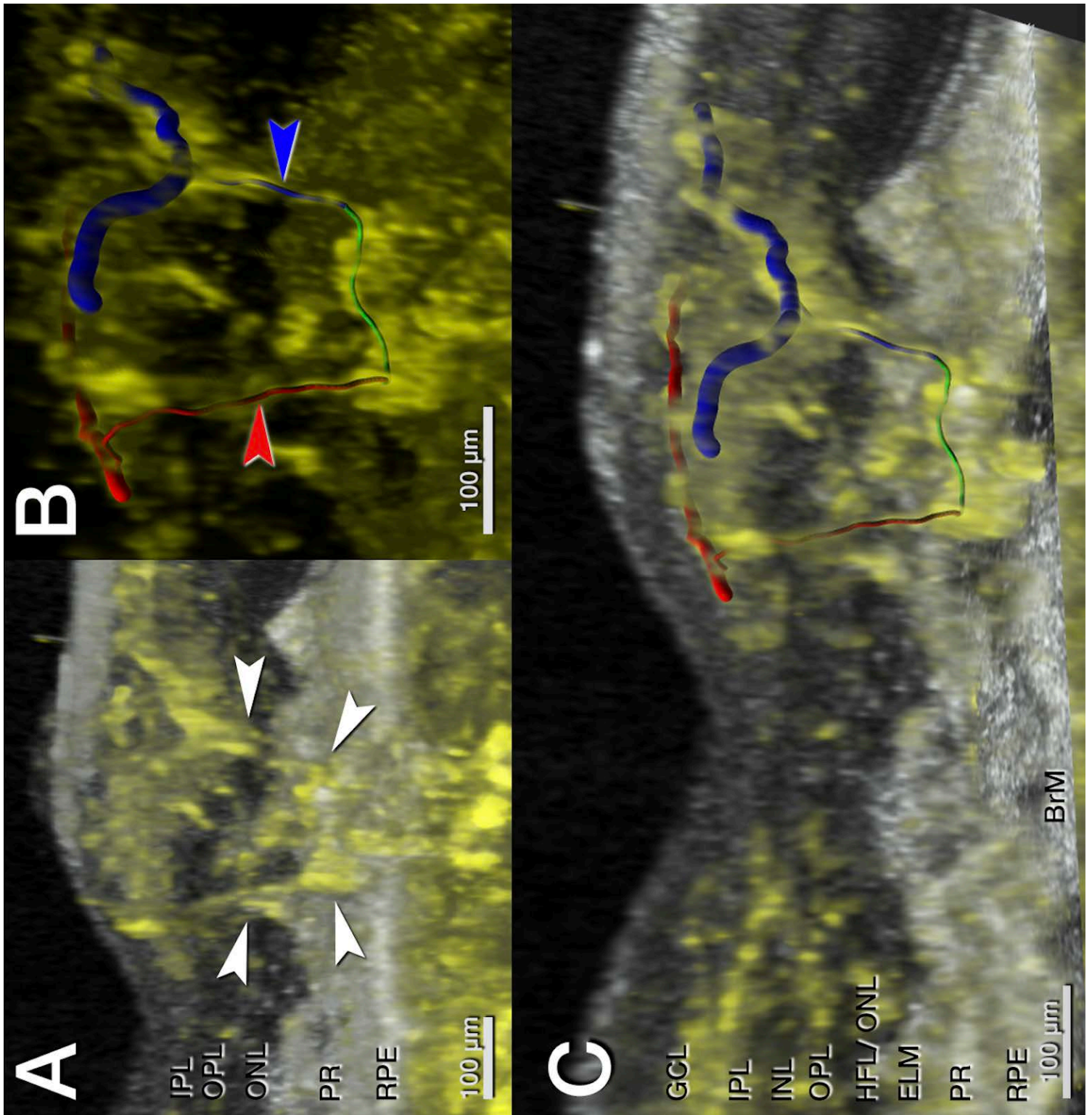


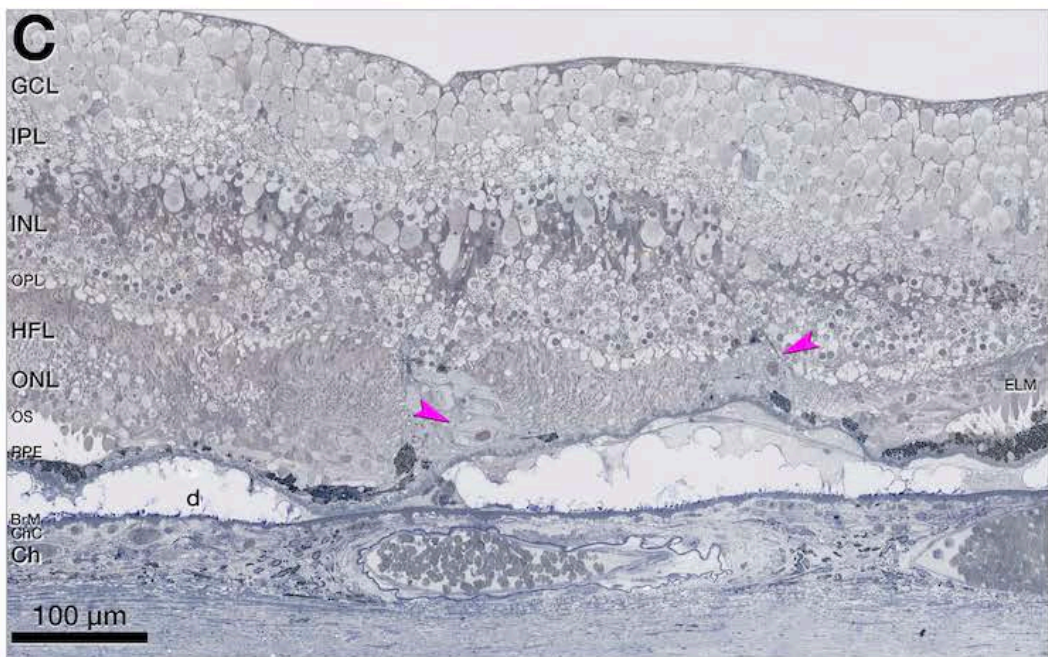
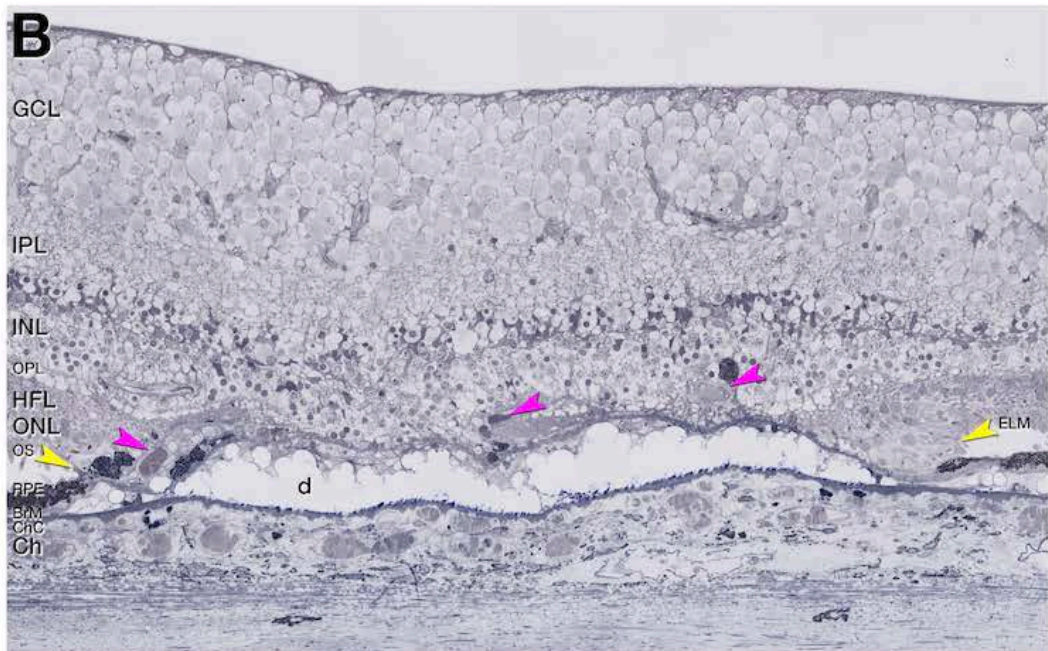
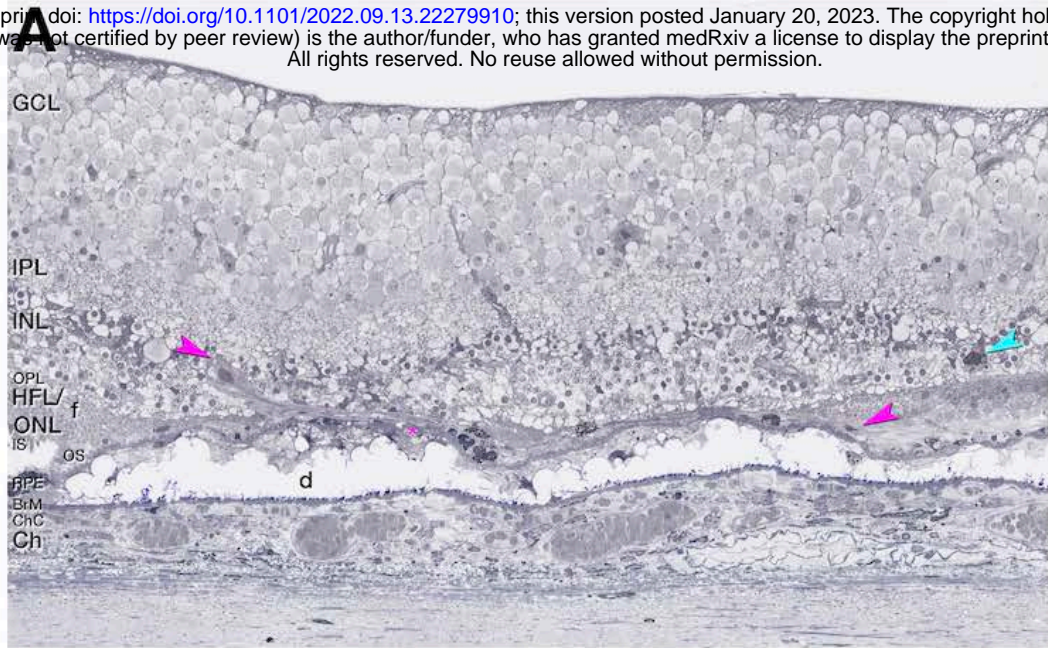


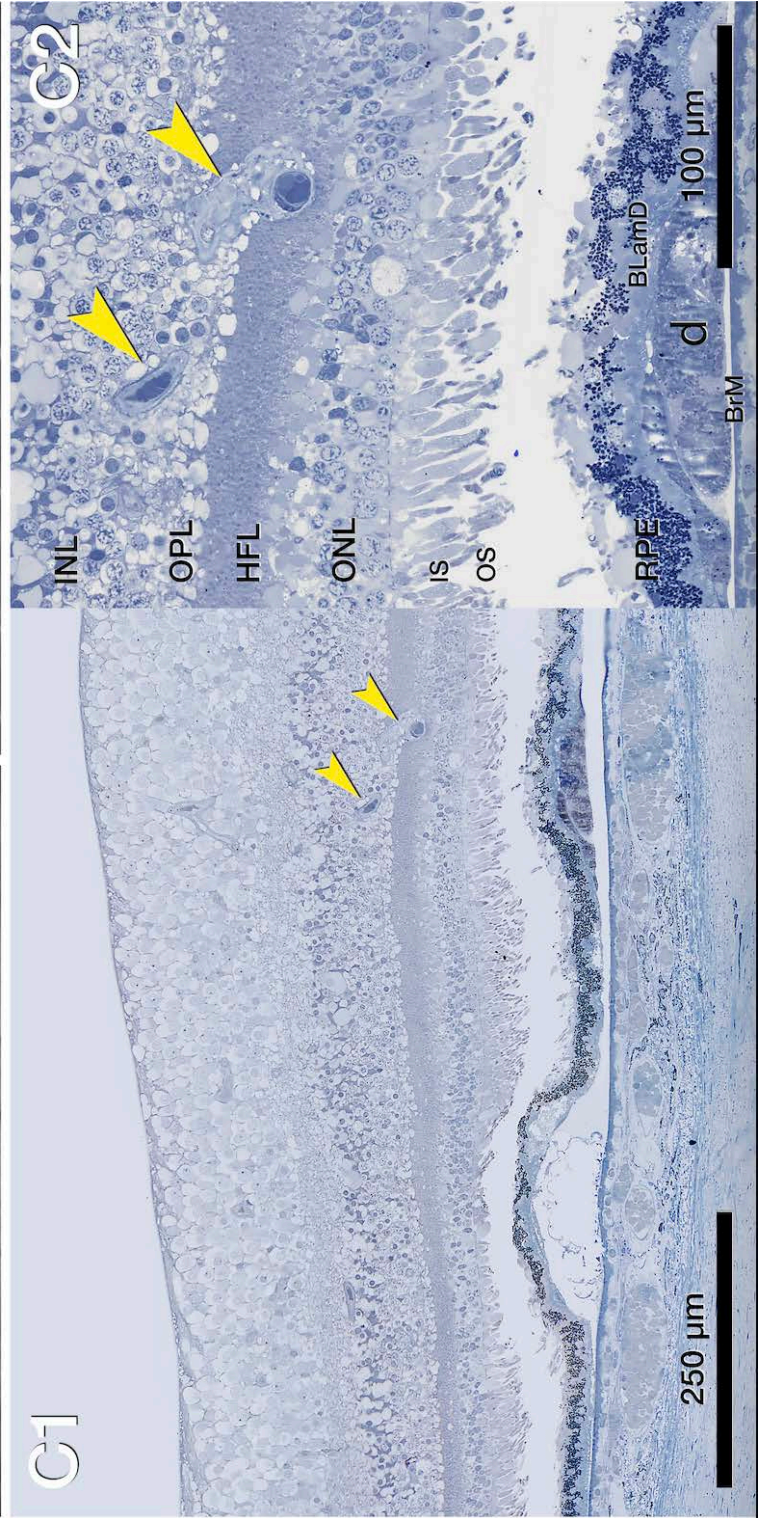
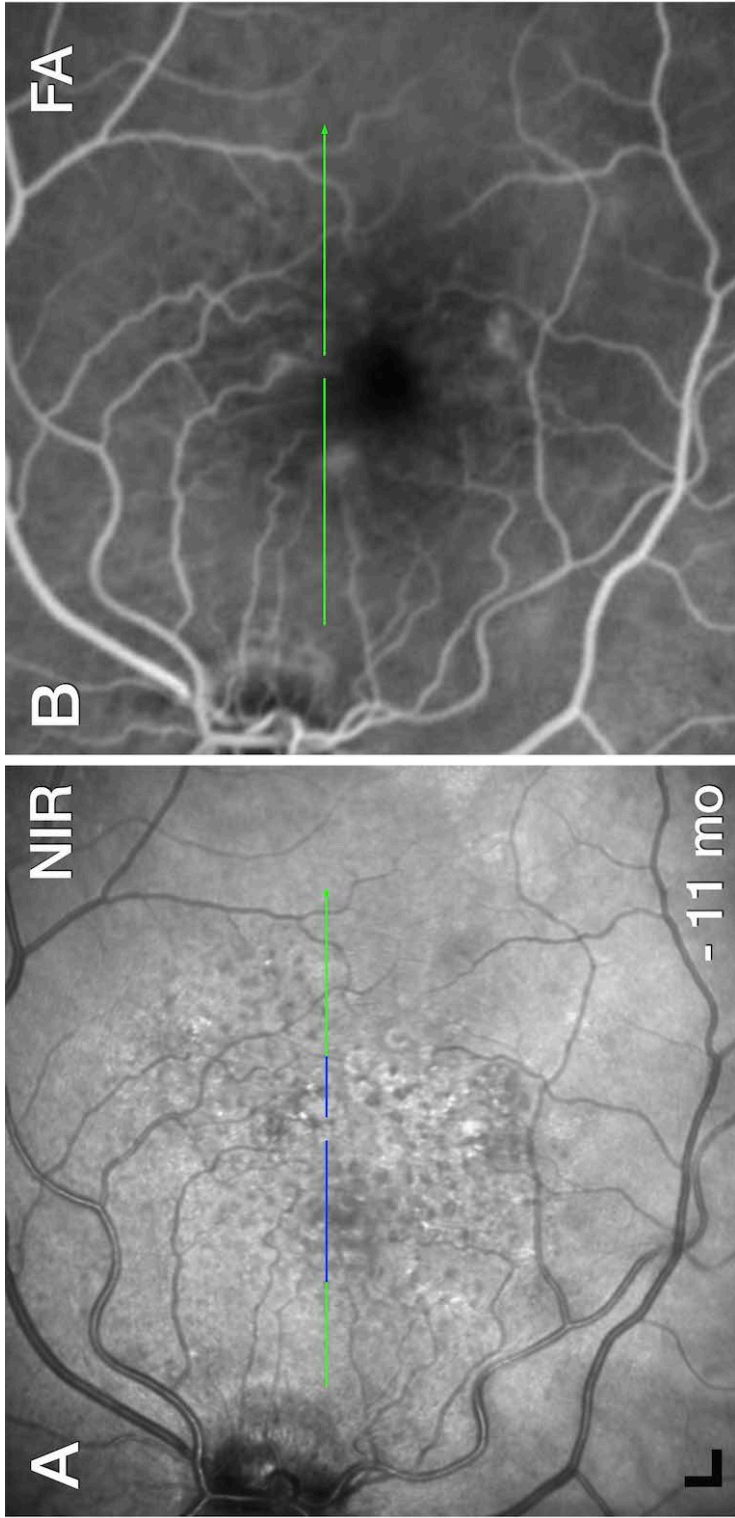


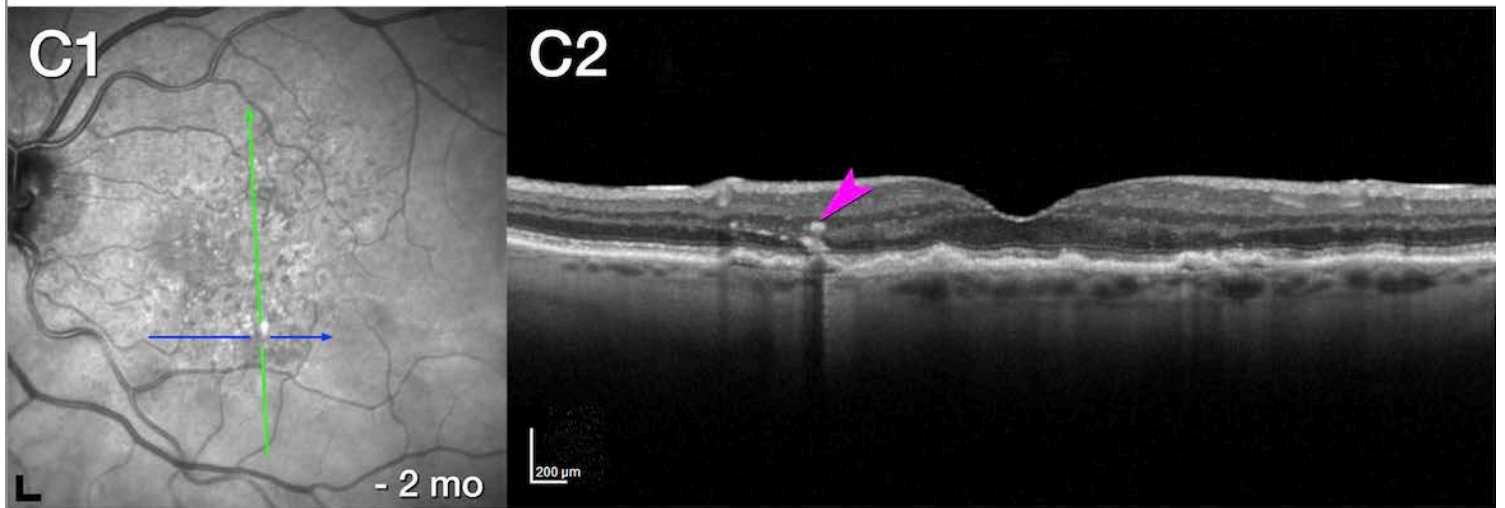
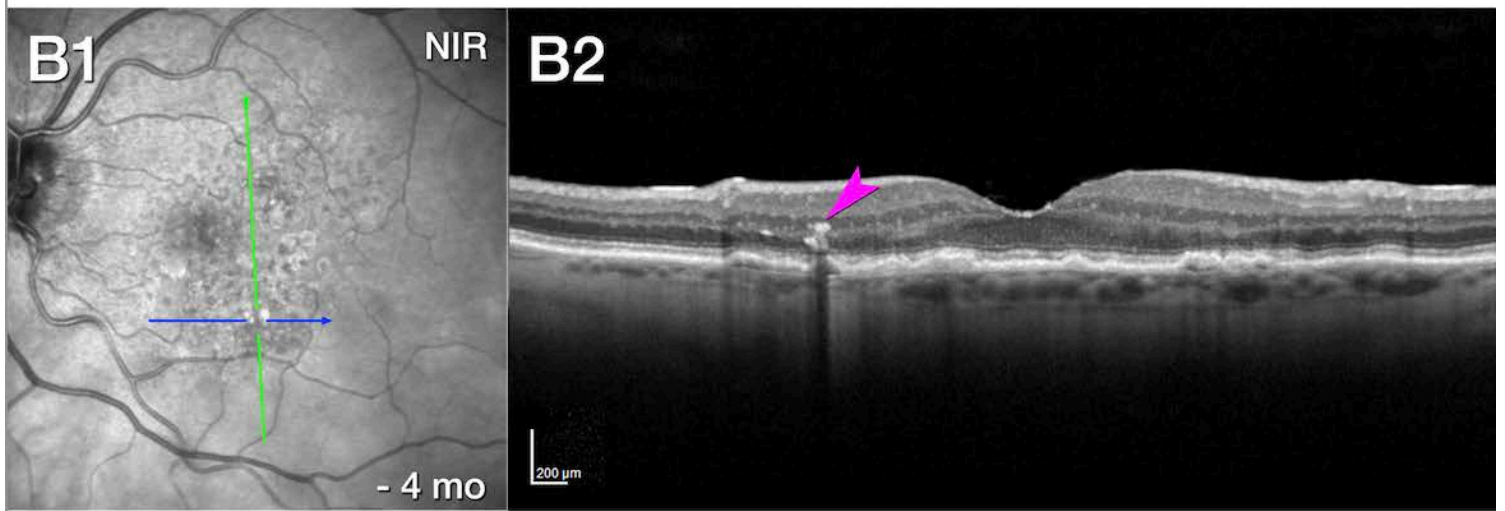
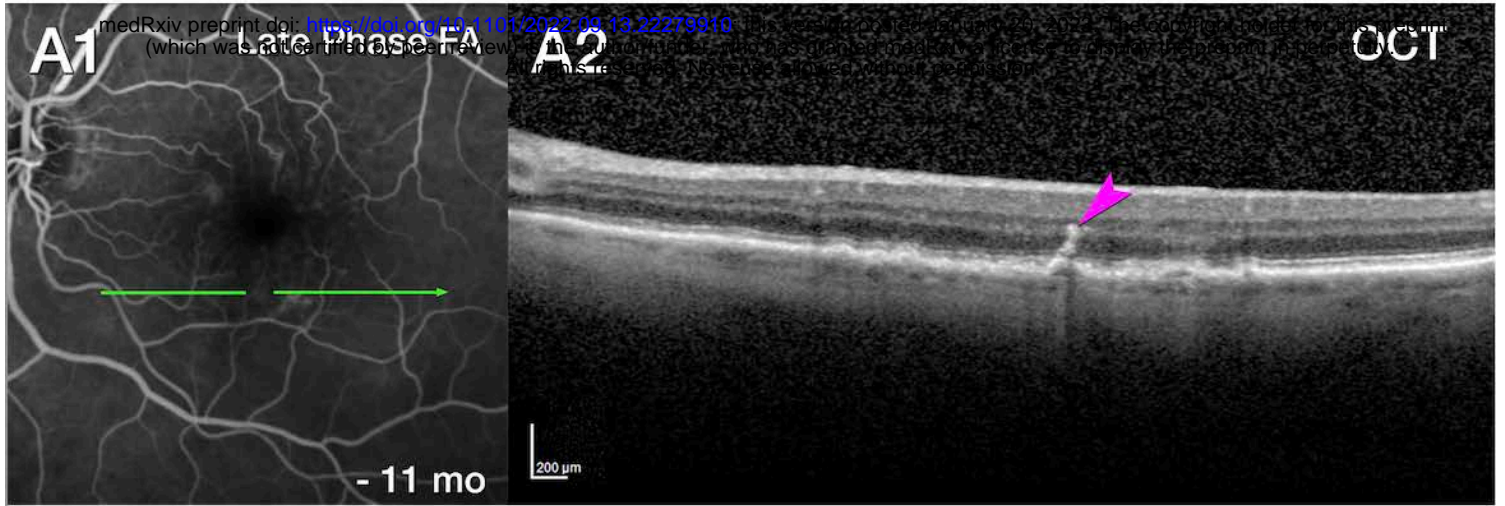


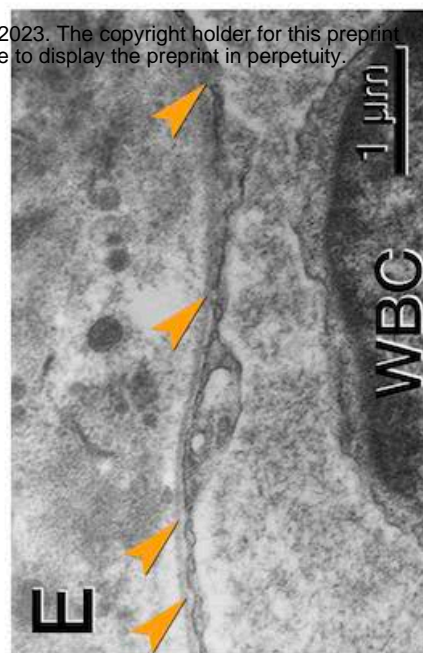
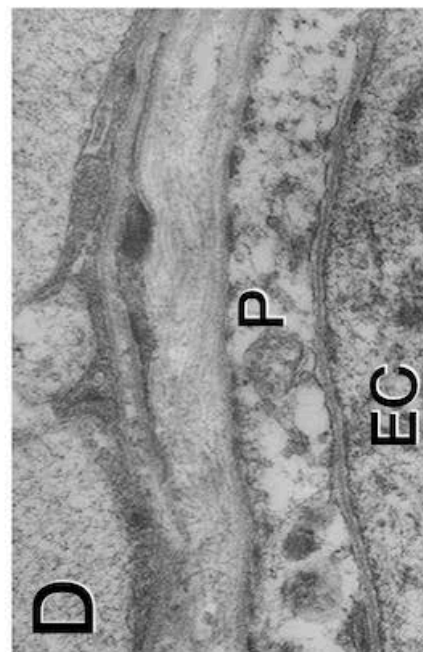
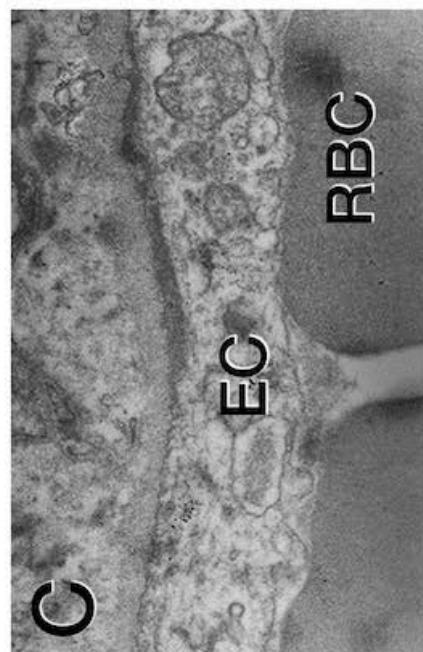
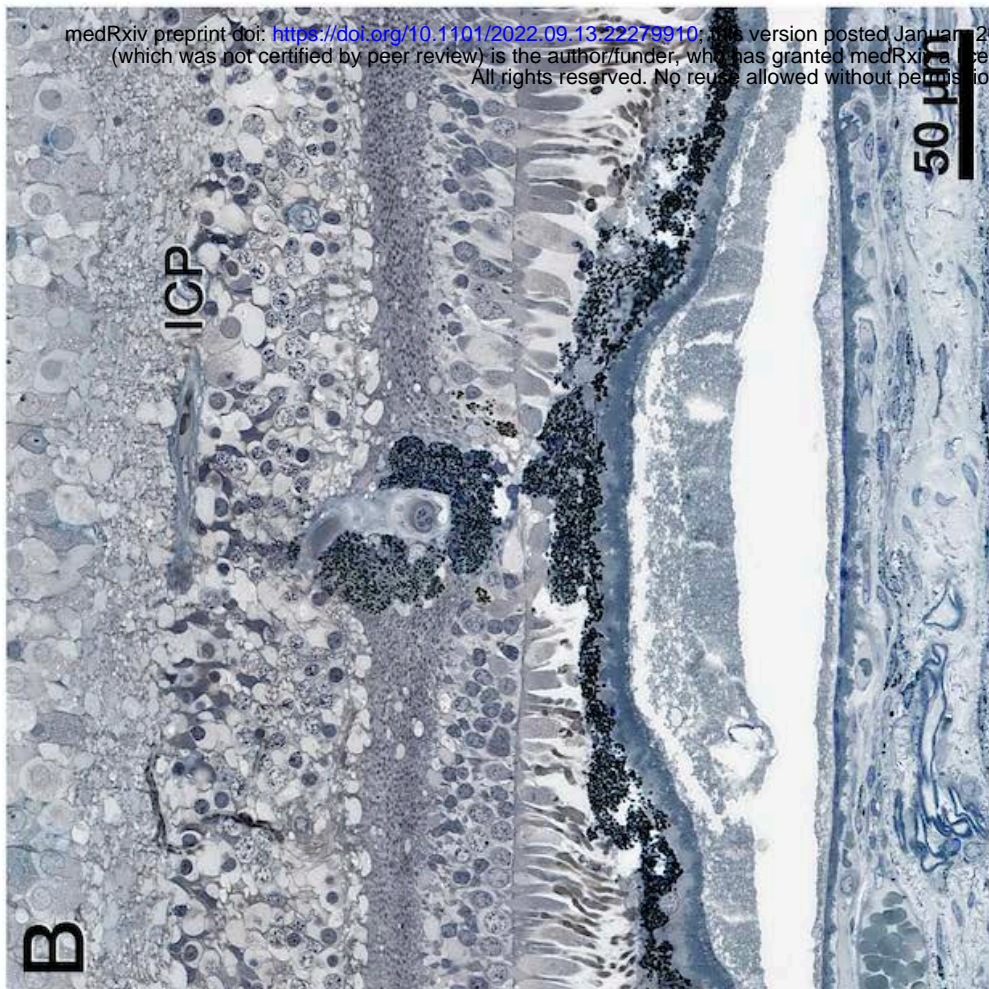
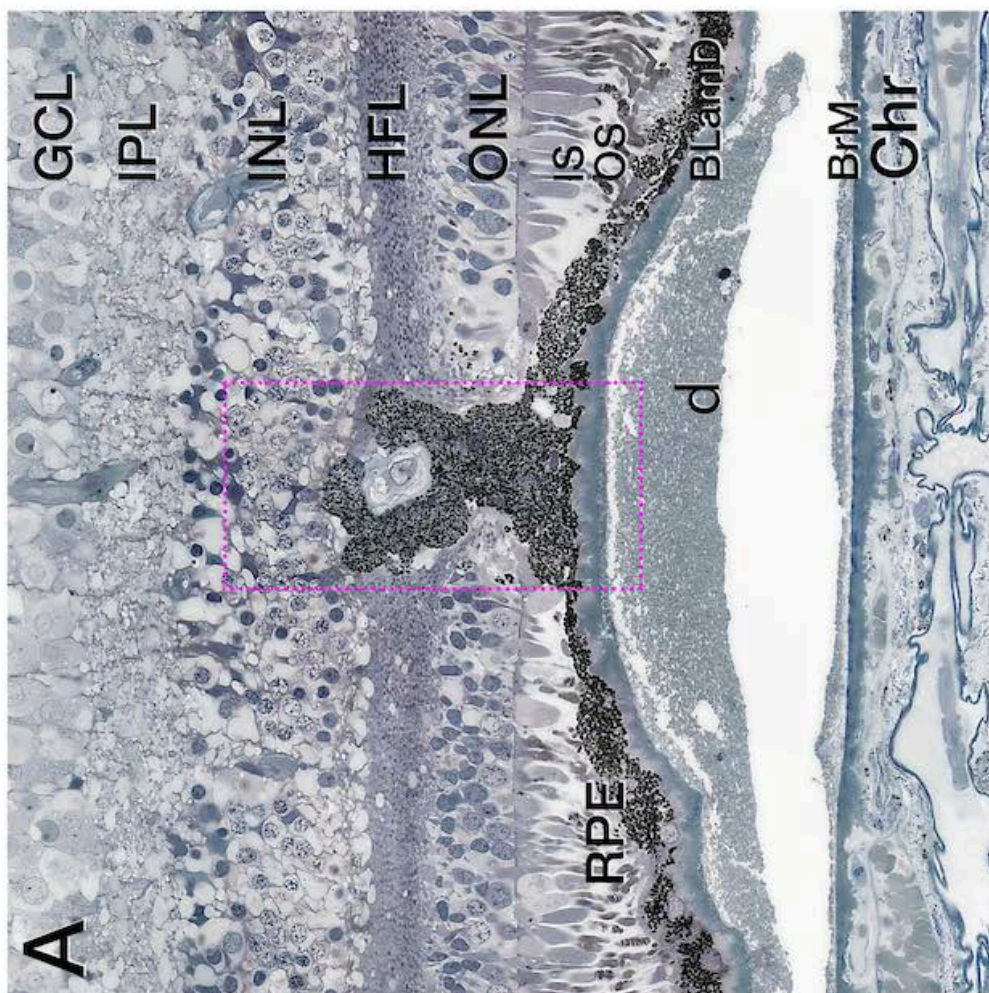


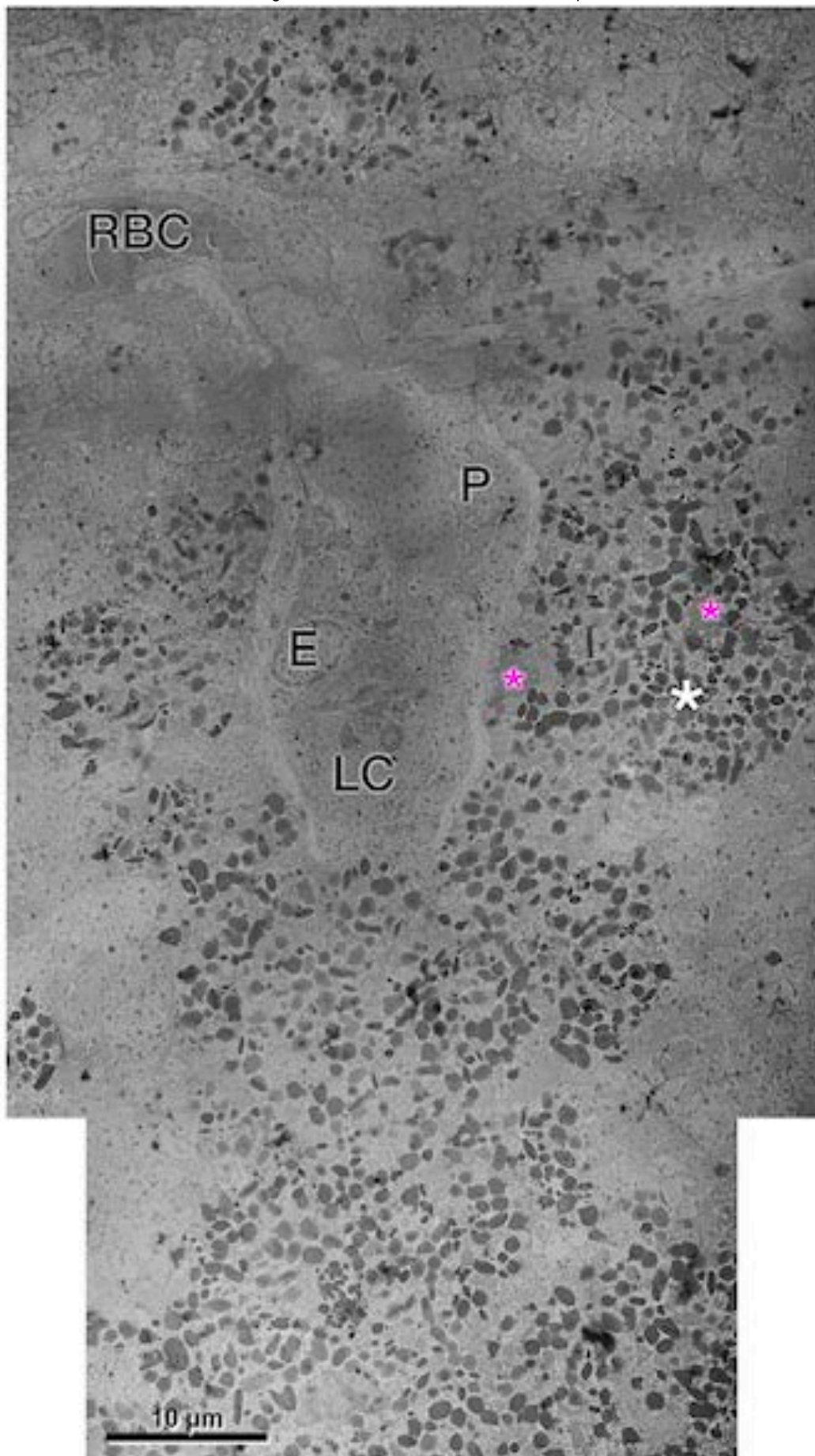


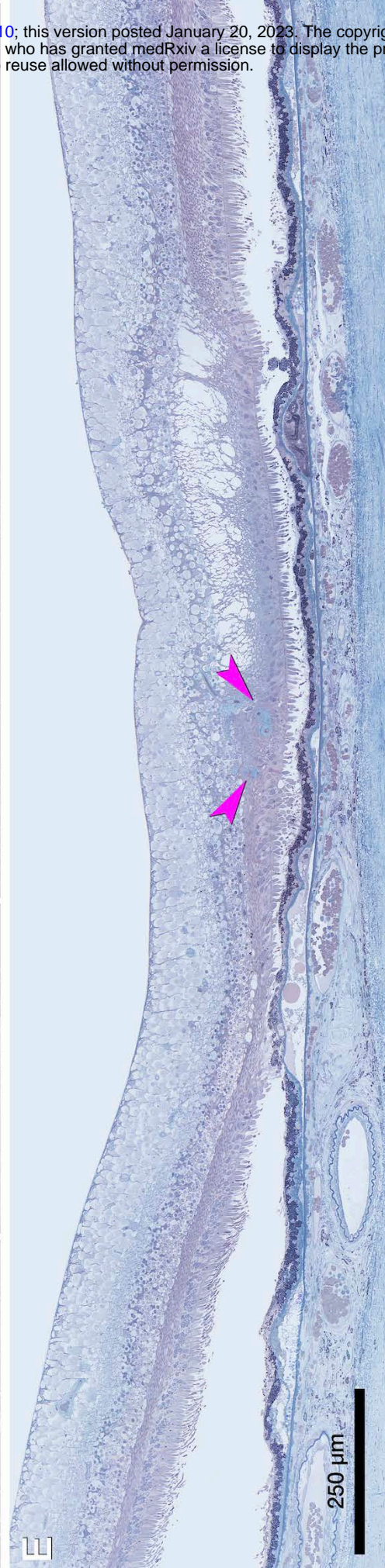
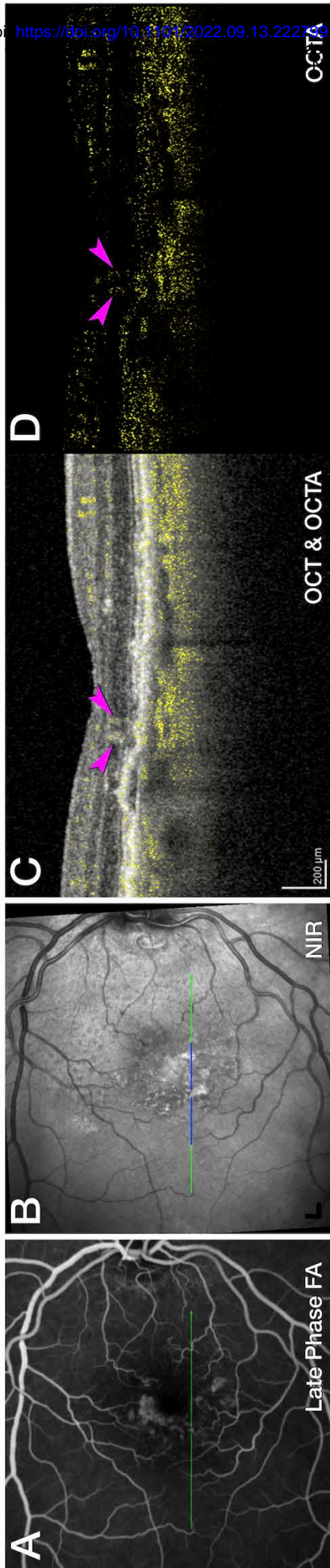


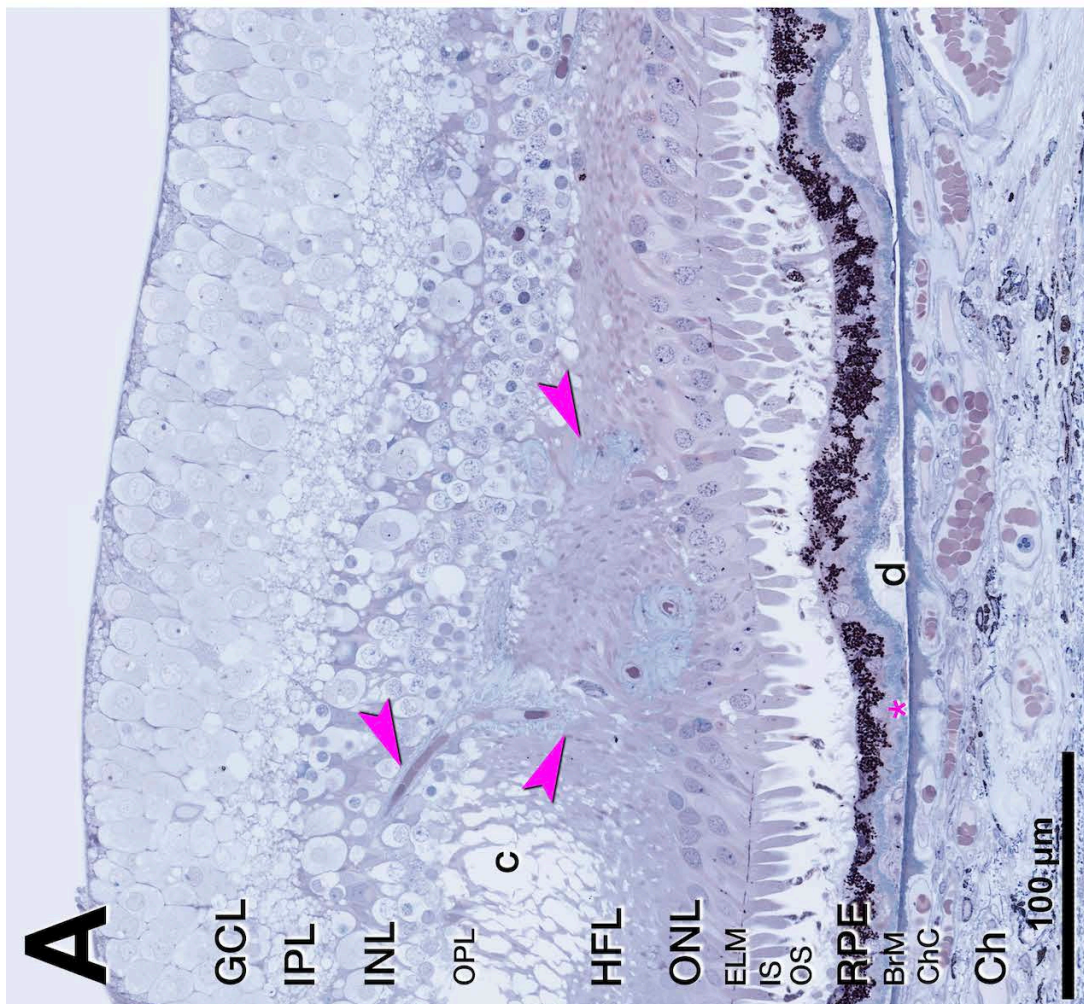
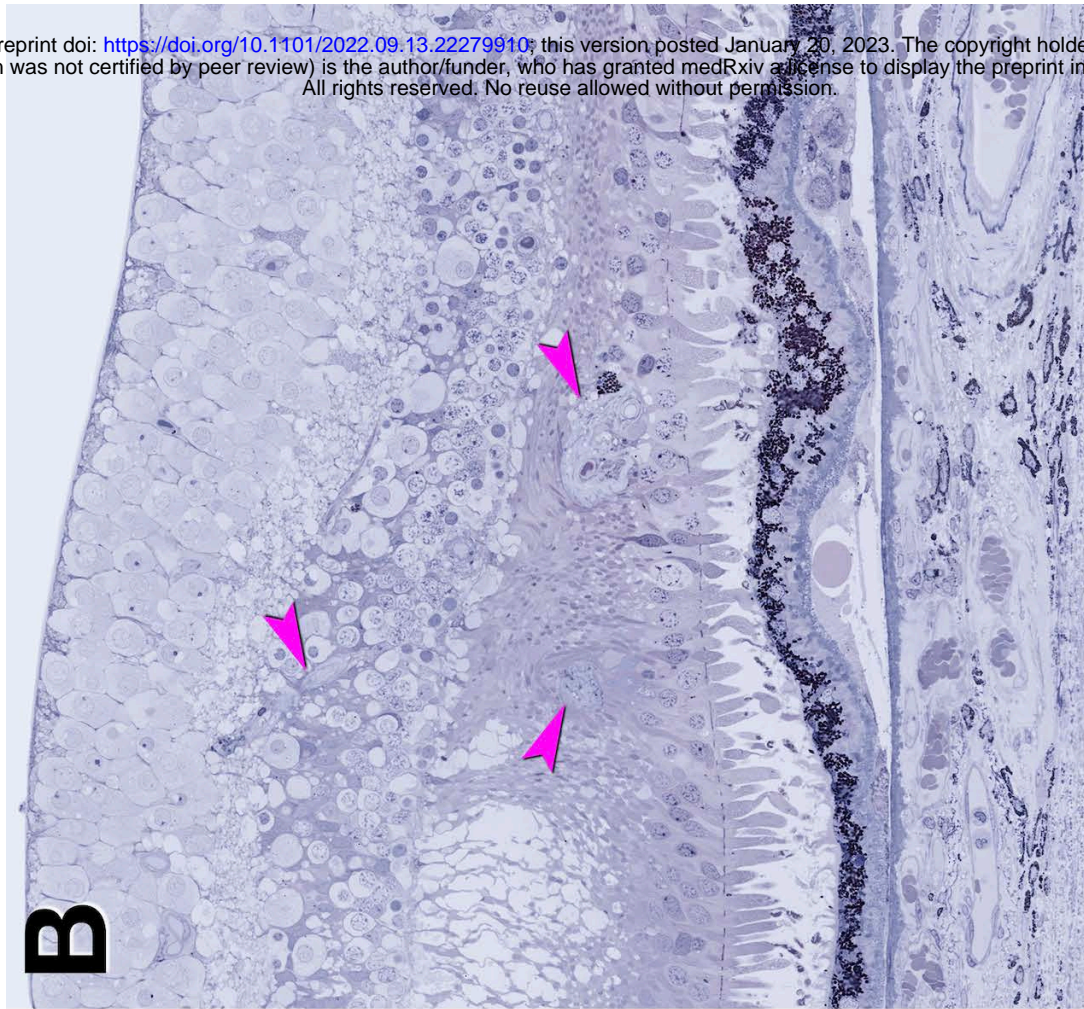














1 **Table S1. Content of imaging data pieces**

figure number as appearing	Laterality and lesion number	Lesion type	Content	Title
<b>1</b>	NA	NA	multimodal imaging	Multimodal retinal imaging of both eyes, 11 months before death
<b>S2</b>	OS2	type 3 MNV	Clinicopathologic correlation, panoramic histology	Hyperfluorescence without histologic correlate, OS2.
<b>S3</b>	NA	NA	clinical imaging baseline	Initial presentation of right eye, 5 years before death
<b>S4</b>	NA	NA	clinical imaging baseline	Initial presentation of left eye, 5 years before death
<b>5</b>	OS4	type 3 MNV	Clinicopathologic correlation, panoramic histology	Multimodal imaging, clinical course, and histology of pyramidal type 3 MNV, OS4.
<b>6</b>	OS4	type 3 MNV	Magnified histology	<u>Pyramidal vascular complex in type 3 MNV, OS4.</u>
<b>7</b>	OS4	type 3 MNV	Transmission electron microscopy	Transmission electron microscopy of pyramidal type 3 MNV, OS4
<b>8</b>	OD1	type 3 MNV	Clinicopathologic correlation, panoramic histology	Multimodal imaging, clinical course, and histology of tangled type 3 MNV, OD1.
<b>S9</b>	OD1	type 3 MNV	3D Volume rendering	Volume rendering of structural optical coherence tomography (OCT, gray) and OCT angiography (OCTA, yellow) of tangled type 3 MNV, OD1.
<b>S10</b>	OD1	type 3 MNV	Magnified histology	Tangled vascular complex in type 3 MNV, OD1.

<b>11</b>	OS1	DRAMA/ type 3 MNV precursor	Clinicopathologic correlation, panoramic histology	Deep retinal age-related microvascular anomaly (DRAMA), OS1.
<b>12</b>	OS3	DRAMA/ type 3 MNV precursor	Clinicopathologic correlation, panoramic histology	Multimodal imaging and histology of deep retinal age-related microvascular anomaly (DRAMA) with intraretinal RPE complex, OS3.
<b>13</b>	OS3	DRAMA/ type 3 MNV precursor	Magnified histology & Transmission electron microscopy	RPE complex associated with deep retinal age-related microvascular anomaly (DRAMA), OS3.
<b>S14</b>	OS3	DRAMA/ type 3 MNV precursor	Transmission electron microscopy	Transmission electron microscopy of DRAMA with RPE complex, OS3.
<b>15</b>	OD3	DRAMA/ type 3 MNV precursor	Clinicopathologic correlation, panoramic histology	Multimodal imaging of deep retinal age-related microvascular anomalies (DRAMAs), OD3.
<b>16</b>	OD3	DRAMA/ type 3 MNV precursor	Magnified histology	Vascular complex of deep retinal age-related microvascular anomaly (DRAMA), OD3.

T3MNV, type 3 macular neovascularization; DRAMA, deep retinal age-related microvascular anomaly; OD, right eye; OS, left eye.

2  
3  
4

**Table 2. Spatial distribution and vascular lesion types in two eyes of the index case.**

Eye, lesion number, color in <a href="#">Fig. 1</a>	ETDRS ring & sector	Lesion type	intravitreal anti-VEGF	Analysis
OD 1 (green)	Inner, S	T3MNV, tangled	37	LM
OD 2 (yellow)	Inner, N	T3MNV, pyramidal	37	LM
OD 3 (fuchsia)**	Inner, T	DRAMA	37	LM
OS 1 (yellow)	Inner, S	DRAMA	6	LM
OS 2 (white)	Outer, I	not found	6	n.a.
OS 3 (fuchsia)	Inner, I	DRAMA	6	LM, EM
OS 4 (green)	Inner, N	T3MNV, pyramidal	6	LM, EM

T3MNV, type 3 macular neovascularization; DRAMA, deep retinal age-related microvascular anomaly; LM, light microscopy; EM, electron microscopy. OD, right eye; OS, left eye.

ETDRS sectors (delimited by 45° lines): S, superior; I, inferior; N, nasal; T, temporal

Within each eye, lesions seen on fluorescein angiography were numbered clockwise, starting at 12:00 (ETDRS grid superior sector).

\* Span width of tangled vascular lesion: 520-769 μm; \*\* pair of vascular lesions.

**Table S3. Diameters of vessels in histology**

**A. External vessel diameter (µm)**

	T3 MNV*			DRAMA*			T3 DCP†	Control†	AMD†
	OD 1	OD 2	OS 4	OS 1	OS 3	OD 3			
Mean	15.02	21.35	12.46	13.39	17.97	8.62	7.18	7.86	6.79
SD	3.81	10.79	0.95	2.68	1.08	1.05	1.11	1.47	1.05

**B. Internal vessel diameter (µm)**

	T3 MNV*			DRAMA*			T3 DCP†	Control†	AMD††
	OD 1	OD 2	OS 4	OS 1	OS 3	OD 3			
Mean	9.34	14.86	9.87	9.40	8.28	5.17	3.69	4.44	3.75
SD	1.85	6.19	0.76	2.00	0.31	0.34	0.92	0.98	0.92

\* 3 to 6 measurements for each; T3 MNV, type 3 macular neovascularization; DRAMA, deep retinal age-related microvascular anomaly.

† 8 female control eyes (84.1 ± 6.7 years; 1 male and 7 female), intermediate AMD eyes (83.4 ± 11.6 years). Histology from Project MACULA <https://projectmacula.org>.

Number of measurements, Type 3 DCP (n=123); Controls (n=88); AMD (n=107).

OS2 no lesion identified in histology.

**Table 4. Features of Type 3 MNV and DRAMA compared**

<b>Feature</b>	<b>Type 3 MNV pyramidal</b>	<b>Type 3 MNV tangled</b>	<b>DRAMA</b>
Location, topographic	ETDRS inner	ETDRS inner	ETDRS inner
Location, layer	HFL/ONL	HFL/ONL	HFL/ONL
RPE	Absent, scattered, migrated	Absent, scattered, migrated	Migrated, intact
ELM	descent	descent	horizontal
Sub-RPE-BL space	End-stages of soft drusen*	End-stages of soft drusen*	Soft drusen, cells
Originating plexus	DCP	DCP	DCP
Shape of vascular complex	Compact, base-down pyramid	Vertical, horizontally spreading	Downward extending loop
Structure over time	dynamic	dynamic	stable <sup>24</sup>
Pericytes	Yes	Yes	Yes
Exudation	Yes	Yes	No
Anti-VEGF response	Yes	Yes	No
Collagenous sheath	Thick	Thin	None/thin if advanced
Endothelium	Non-fenestrated	Non-fenestrated	Non-fenestrated

\*Calcific nodules, cells (subducted RPE, macrophages, giant cells, fibroblasts), Müller glia, avascular fibrosis  
Based on current and published data.<sup>3, 16, 24</sup>